Initiation of the Western Pacific Warm Pool at the Middle Miocene Climate Transition?

S.M. Sosdian* **& C. H. Lear**
School of Earth and Ocean Sciences, Cardiff University, Main Building, Park Place, Cardiff, CF10 3AT

*Corresponding author

Abstract

Across the middle Miocene, Earth's climate underwent a major cooling and expansion of the Antarctic ice sheet. However, the associated response and development of the tropical climate system is not fully understood, in part because this is influenced by both global climate and also low latitude tectonic gateways and paleoceanography. Here we use combined $\delta^{18}O$ and Mg/Ca of planktic foraminifera to reconstruct the thermal history and changes in hydrology from the Indo-Pacific region from 16.5 to 11.5 Ma. During the warmth of the early middle Miocene, our records indicate a dynamic ocean-atmosphere system in the Indo-Pacific region, with episodes of saltier and warmer tropical surface waters associated with high pCO_2 and retreat of the Antarctic ice sheet. We show that across the middle Miocene Climate Transition (MMCT) surface ocean temperatures in the Indo-Pacific cooled by ~ 2˚C, synchronous with the advance of the Antarctic ice sheet. The associated cooling in the Southern Ocean appears to have started earlier, and was stronger. Further, we show that western Pacific Ocean warmed and eastern tropical Indian Ocean freshened following the MMCT, likely caused by the constriction of the Indonesian Seaway and reduced connectivity between the Pacific and Indian Oceans following Antarctic glaciation. The MMCT therefore represented a key phase in the evolution of the West Pacific Warm Pool and associated tropical climate dynamics.

Keywords: Miocene, Tropics, Mg/Ca, planktic foraminifera, glaciation, Indo-Pacific

Key Points:

- Low latitude Indo-Pacific sea surface temperatures cooled synchronous with the advance of the Antarctic ice sheet
- Eastern Tropical Indian Ocean freshened following the Middle Miocene Climate Transition
- Sea level fall and changing paleogeographic conditions constricted the Indonesian Seaway modifying the Tropical Indian Ocean climate and warming the western Pacific ocean.

For resubmission to ***Paleoceanography, Special Issue on the Miocene***

1. Introduction & Background

Across the Middle Miocene, the Earth's climate gradually changed from a period of global warmth and retreat of the Antarctic ice sheet known as the Miocene Climatic Optimum (MCO;~17-14.7 Ma) to a cooler climate with regrowth of the Antarctic ice sheet at the Middle Miocene Climate Transition (MMCT), exhibited by an stepwise increase in the benthic foraminiferal oxygen isotope record (14.2-13.9 Ma). Global warmth and high carbon dioxide (CO_2) levels were pervasive during the MCO, with global surface temperature perhaps > 7°C than present (Shevenell et al., 2004; Lewis et al., 2007; Verducci et al., 2007; Kuhnert et al., 2009; Majewski & Bohaty, 2010; Levy et al., 2016; Super et al., 2018; Hartman et al., 2018; Sangiorgi et al., 2018). Following the MCO, CO_2 decreased from ~580-670 ppm to 380-420 ppm, and the Antarctic ice sheet re-advanced, causing a sea level fall of several tens of metres (Lear et al., 2010, John et al., 2011; Foster et al., 2012, Badger et al., 2013; Sosdian et al., 2018). Understanding the driving mechanisms of this major step in Earth's climate evolution where the Antarctic ice sheet transitioned from a wet-based to dry based ice sheet (i.e. more modern like ice sheets) (Lewis et al., 2007) is critical to understand the interactions between carbon cycle, cryosphere and climate change. Existing records demonstrate large scale cooling in regions proximal to Antarctica and the North Atlantic (Shevenell et al., 2004; Lewis et al., 2007; Verducci et al., 2007; Kuhnert et al., 2009; Majewski & Bohaty, 2010; Levy et al., 2016; Super et al., 2018; Hartman et al., 2018; Sangiorgi et al., 2018), reorganization of polar frontal systems (Verducci et al., 2007; Kuhnert et al., 2009), and intensification of equatorial upwelling and overturning circulation (Holbourn et al., 2013; 2014). For example, the continuous, orbitally-resolved Mg/Ca-sea surface temperature (SST) and planktic isotope record from the Pacific sector of the Southern Ocean shows a 6 to 7°C cooling and freshening preceding the main glaciation step by 300 kyr (Shevenell et al., 2004), although non-thermal effects (e.g., pH, dissolved inorganic carbon) on Mg/Ca must be considered and warrant caution when interpreting the nature and extent of cooling (Gray & Evans, 2019; Holland et al., 2020). The timing of these changes has led to the idea that meridional heat/moisture transport and an early thermal isolation of the Antarctic continent played a fundamental role in triggering ice growth (Shevenell et al., 2004). Recent Antarctic ice-proximal reconstructions (e.g., Sangiorgi et al., 2018) have shown sea ice expansion, increasing SST gradients and cooling of ice-proximal surface waters across the MMCT hinting at a northward shift in the Southern Ocean frontal system. As most SST records are derived from circum-polar regions, it is difficult to determine the global climatic signature of the MMCT and identify the role of Southern Ocean processes, carbon cycle, or oceanographic changes (Shevenell et al., 2004; Verducci et al., 2007; Kuhnert et al., 2009; Super et al., 2018; Sangiorgi et al., 2018). Records from both high and low latitude sites are

necessary to mechanistically understand the cause and effects of this key climate transition and test proposed hypotheses.

The middle Miocene also witnessed important changes in the tectonic configuration of low latitude ocean seaways, which must be considered when interpreting records of tropical sea surface temperature and hydrology. Low latitude tectonic events (e.g. Panamanian and Indonesian Seaway constriction) could affect the distribution of heat between ocean basins and reorganize tropical surface ocean structure and climate patterns (Gourlan et al., 2008; von der Heydt & Dijkstra, 2011; Hamon et al., 2013; Bialik et al., 2019). In the present day, the Indonesian Throughflow transports the warm waters of the Western Pacific Warm Pool (WPWP) and excess heat and freshwater through a series of straits and shallow seas eventually entering and warming the Indian Ocean. This heat export affects ocean-atmosphere coupling in the tropical Pacific and Indian Oceans with implications for the development of Indian Ocean Dipole events and changes in global atmospheric circulation patterns (Schneider, 1998; Wajsowicz and Schneider, 2001; Sprintall, 2003).

On geological timescales the long-term drift of Australia towards Asia has progressively changed the structure of this seaway. From the late Oligocene to the early Miocene, the Indonesian seaway became a shallow water throughflow effective for surface water transport while the transport of deep water between the deep oceans diminished (Kuhnt et al., 2004). Early biogeographic studies of discrete time slices (22, 16, 8 Ma) suggested tectonic closure of the Indonesian seaway as a trigger for invigoration of tropical surface ocean circulation systems in the middle Miocene (Kennett et al., 1985), although tectonic reconstructions suggest that the Indonesian seaway became restricted before the middle Miocene (Ali et al., 1994; Hall, 1996; 2002). Further, the deeper and more open Indonesian seaway could impact the position of the WPWP, with a Miocene warm pool residing in the eastern Indian Ocean (von der Hedyt & Dijkstra, 2011). This suggests a pivotal role for the seaway in setting the climate budget of the Indo-Pacific region, proximal seas and distal outflow locations in the Miocene Tropical Indian Ocean.

To unravel the relative roles of paleogeography, CO_2, and glaciation in middle Miocene climate, equatorial surface ocean temperature records are required. However, documentation of low-latitude conditions is limited both spatially and temporally, and a deeper understanding awaits development of records comparable to those available from the Southern Ocean. Oxygen isotope records from the equatorial Pacific region show a warming across the middle Miocene, however confident interpretation of these records is difficult due to likely diagenetic overprints (Savin et al. 1985; Stewart et al. 2004). Orbital scale Mg/Ca-derived sea surface temperature (SST) and oxygen isotope ($\delta^{18}O$) records from the South China Sea (SCS) show

dynamic changes in tropical hydrology (i.e. warming and freshening) in response to Antarctic glaciation suggesting a role for large shifts in the Intertropical Convergence Zone (ITCZ) position (Holbourn et al. 2010). In contrast, low resolution alkenone-derived SST reconstructions from the Eastern Equatorial Pacific (EEP) shows a cooling event across the MMCT (Rousselle et al. 2013), although this record is difficult to interpret due to proxy saturation during the warm MCO, prior to the MMCT. In the eastern tropical Indian Ocean, Sosdian et al. (2020) show that SSTs in this region cooled along with the MMCT. These lines of evidence suggest that the MMCT was associated with a climate reorganization event in the low latitudes, however, additional records are needed to resolve the roles of CO_2, glaciation, and paleogeography in context of tropical climate evolution.

Here we present records of surface ocean hydrographic conditions derived from combined planktic foraminiferal Mg/Ca and oxygen isotope ($\delta^{18}O_p$) data from Ocean Drilling Program (ODP) Site 806 located in the western equatorial Pacific Ocean and $\delta^{18}O_p$ record from ODP Site 761 from the eastern tropical Indian Ocean. The climate records span the time period from 16.5 to 11.5 Ma and allow us to explore regional versus global changes in climate. We further use the combined Mg/Ca and $\delta^{18}O_p$ from surface dwelling planktic foraminifera to reconstruct the oxygen isotope composition of seawater ($\delta^{18}O_{sw}$) in order to evaluate temporal changes in tropical surface ocean salinity across the middle Miocene. Overall we find that the Indo-Pacific cooled across the MMCT in step with Antarctic glaciation. Further, we show that the Indian Ocean freshened relative to the Pacific and western equatorial Pacific warmed following this transition likely caused by the constriction of the Indonesian Seaway. The Middle Miocene Climate Transition therefore likely represented a key phase in the evolution of the West Pacific Warm Pool and associated tropical climate dynamics.

2. Materials & Methods

2.1 Age models and oceanographic settings of study sites

2.1.1 ODP Site 806B – western equatorial Pacific Ocean

Ocean Drilling Program (ODP) Site 806B (2520 m water depth, 0°19.1'N, 159°21.7'E; Fig. 1) is located on the Ontong Java Plateau in the western equatorial Pacific and has relatively high sedimentation rates (20-30 m/Myr) with a complete Miocene section of carbonate ooze. A 5° latitudinal northward drift of the Ontong Java Plateau since the Middle Miocene puts this site in a tropical location during the present day (~5˚S; Figure S1). This study uses sediment samples from cores 43 to 60 (400–566 metres below seafloor (mbsf)), with a temporal resolution of ~130 kyr during the study interval (16.5 to 11.5 Ma). We use the age model of Lear et al., (2015) which is a fourth order polynomial fit through nannofossil and

planktic foraminiferal biostratigraphical events at ODP 806B on the Berggren et al., (1995) timescale for new planktic Mg/Ca presented here and previously published oxygen isotope records (Corfield & Cartlidge, 1993; Nathan & Leckie, 2009; Lear et al., 2015). The benthic oxygen isotope ($\delta^{18}O_b$) data from Holbourn et al. (2013) are presented on the Lear et al., (2015) age model.

ODP Site 806 is today located in the warm waters of the WPWP, due to the buildup of warm waters trapped in front of the Indonesian archipelago (Figure 1). Here, the modern day thermocline is deep and surface waters exceed 29°C, with a small range of ~29- 29.5°C. Since at least the early Miocene, ODP Site 806 has remained in western Pacific equatorial waters (Sclater et al., 1985). On interannual timescales, the El Niño Southern Oscillation shoals the thermocline and lessens the precipitation in the WPWP. Due to its location, good core recovery, and preservation of microfossils, ODP Site 806 is an ideal location to examine the thermal stability over wide range of timescales (i.e. kyr-Myr) of the western equatorial Pacific region.

2.1.2 ODP Site 761B – eastern tropical Indian Ocean

ODP Site 761 was cored in 2179 m water depth on the Wombat Plateau, off northwest Australia (16° 44.23′ S, 115° 32.10′ E ; Fig. 1). A 10-15° latitudinal northward drift of Australia since the Middle Miocene puts this site in a subtropical to tropical location during the present day (~21˚S; Scotese et al., 1988; Figure S1). The continuously cored Neogene section studied here extends between 35 and 50 mbsf and slow sedimentation rates have led to unusually shallow burial depths (<50 m) for the middle Miocene sequence, leading to enhanced foraminiferal preservation. 20 cc sediment samples were taken at approximately 10 cm resolution, resulting in average temporal resolution of ~23 kyr for planktic foraminiferal stable isotopes. Previously published benthic foraminiferal stable isotope and planktic foraminiferal Mg/Ca data exist at this site with an average temporal resolution of 17 and 23 kyr respectively (Holbourn et al., 2004; Lear et al., 2010; Sosdian et al., 2020). We use the age model of Lear et al., (2010) which is a fourth order polynomial fit through the biostratigraphic and isotopic datums provided by Holbourn et al. (2004) on the Berggren et al. (1995) timescale. Surface salinity estimates from nearby sites are 34.5 (GLODAP; Key et al., 2004).

ODP Site 761 sits in the midst of a dynamic hydrographic regime in the eastern Indian Ocean. During the austral winter, a subtropical high occupies the site and dry easterly winds blow over the Australian continent and into the Indian Ocean. During the austral summer, the subtropical high moves poleward and the ITCZ penetrates further south delivering monsoonal rain. Seasonal temperatures range from 30.9°C in the austral summer to 25.3°C in the austral winter with mean annual temperatures around 28°C. Since the middle Miocene, it has been proximal to the western edge of the present day Indonesian throughflow, which transports cool, low salinity North Pacific thermocline water to the Indian Ocean. Additionally it is directly under the influence of the modern Leeuwin Current, a narrow, shallow current that transports warm, low-salinity, nutrient-deficient water southward along the west coast of Australia (Pattiaratchi, 2009; Gallagher et al., 2009), derived from water formed within the Indonesian Throughflow and the Central Indian Ocean (Wijffels et al., 2002; Domingues et al., 2007). Surface salinity estimates from nearby sites are 34.15 (GLODAP; Key et al., 2004).

2.2 Mg/Ca and $\delta^{18}O$ Analysis

Between 20-30 tests of planktic foraminifera *Dentoglobigerina altispira* and 30-40 tests of the planktic foraminifera *Trilobatus trilobus* were picked from the 300-355 μm size fraction at ODP Sites 806 and 761, respectively. The picked specimens were weighed and crushed between plates and homogenized for analysis. In some samples (~25 out of 229 samples), where planktic foraminifera abundance was low, fewer specimens (10-20 individuals) were analyzed. The Mg/Ca and $\delta^{18}O_p$ data were generated from splits of the same samples after initial homogenization of crushed tests. Mg/Ca data for ODP Site 761 were previously published in Sosdian et al., (2020), in this study we also present the $\delta^{18}O_p$ data from the same samples.

Test fragments for Mg/Ca analyses were cleaned using a protocol to remove clays and organic matter (Barker et al., 2003). Between the clay removal and oxidative steps the samples were examined under a binocular microscope, and non-carbonate particles were removed using a fine paintbrush. Samples were dissolved in trace metal pure 0.065M HNO_3 and diluted with trace metal pure 0.5M HNO_3 to a final volume of 350 μl. Samples were analyzed at Cardiff University on a Thermo Element XR ICP-MS against standards with matched calcium concentration to reduce matrix effects (Lear et al., 2002). Mg/Ca data for a sample was rejected when Al/Ca exceeded 80 μmol/mol and/or Fe/Mg>1. Cleaning effectiveness was supported by uncorrelated Mg/Ca, Fe/Ca, and Mn/Ca. Long term precision as determined by analyzing an independent consistency standard during each run for one year is ~0.5% (r.s.d.) for Mg/Ca.

Stable oxygen and carbon isotope ratios were measured at Cardiff University on a Finnigan MAT 252 micro-mass spectrometer Kiel III Carbonate Device when sample weights were less than 100 μg and measured on a Delta isotope ratio mass spectrometer when samples were greater than 100 μg. Analytical errors based on replicate measurements of a laboratory standard (NBS 19) are 0.08‰ for $\delta^{18}O$ (2σ).

2.4 Planktic Foraminiferal Taxonomy and Ecology

At ODP Site 806, the abundant *D. altispira* is an ideal species to reconstruct SST in the western equatorial Pacific as it is a near-surface dweller, and common in tropical waters (Fig. S2; Corfield & Cartlidge, 1992). *D. altispira* evolved in the late Oligocene and became extinct in the late Pliocene (Kennett & Srinivasan, 1983 Gasperi & Kennett, 1992, 1993; Chaisson & Leckie, 1993; Norris et al. 1993). Comparison of isotope records of a typical planktic foraminiferal assemblage in the western equatorial Pacific shows that *D. altispira* behaves as a shallow water species for the middle Miocene, and probably harbors symbionts similar to contemporeanous *T. trilobus* (Pearson, 1995).

In the modern ocean, *T. trilobus* is considered to be a morphospecies of *T. sacculifer*, although *T. sacculifer* did not evolve until the Pliocene (Figure S2; Kennett & Srinivasan, 1983; Spezzaferri et al., 2015). *T. trilobus,* a multi-chambered and symbiont-bearing species, is predominantly a mixed layer dweller calcifying at 0-50m and is abundant in subtropical to tropical oceans. Numerous studies have successfully used this foraminiferal species to study low latitude surface processes in the Quaternary and Neogene time periods (e.g., Elderfield & Ganssen, 2000; Wara et al., 2005; Badger et al., 2013). At ODP Site 761, *T. trilobus* is abundant throughout the middle Miocene and thus is an ideal species to estimate SSTs (Zachariasse, 1992). Studies have shown that temperatures derived from *T. sacculifer* are most suitable for estimating annual mean SST in tropical waters, between 20° N/S within ±1˚C (Anand et al., 2003; Fraile et al., 2009; Sosdian et al., 2020).

2.5 Mg/Ca-paleotemperature relationship and non-thermal influences

Test Mg/Ca and calcification temperature in planktic foraminifera show an exponential relationship across a range of modern day surface ocean temperatures deduced from core-top, culturing and sediment trap studies (Dekens et al., 2002; Anand et al., 2003; Duenas-Bohorquez et al., 2011). The exponential constant that describes the temperature sensitivity (A in equation 1) ranges from 0.070 to 0.113 determined from a wide range of modern planktic species (Elderfield and Ganssen, 2000; Rosenthal and Lohmann, 2002; Anand et al., 2003; Cleroux et al., 2008; Regenberg et al., 2009).

$$Mg/Ca_{foram} = Be^{AT} \quad \text{(eq. 1)}$$

Accurate reconstructions of Miocene sea surface temperatures derived from planktic Mg/Ca ratios requires consideration of variations in seawater Mg/Ca.

$$\frac{Mg}{Ca}_{foram} = \left[\frac{\frac{Mg}{Ca}_{sw}(t)}{\frac{Mg}{Ca}_{sw}(0)}\right]^{C} Be^{AT} \quad \text{(eq. 2)}$$

where $Mg/Ca_{sw}(t)$ and $Mg/Ca_{sw}(0)$ are seawater Mg/Ca ratios for the Miocene and present respectively and A, B, and C are constants (A=exponential, B=pre-exponential, C=power law constant). Mg and Ca have relatively long residence times (~13 Myr and ~1 Myr respectively) in the ocean (Broecker and Peng, 1982). Changes in weathering, hydrothermal activity, and carbonate deposition could lead to secular changes in Mg/Ca_{sw}. Seawater Mg/Ca values are independently estimated from a range of proxies (fluid inclusions, calcite veins, echinoderm, paired Mg/Ca-clumped isotope measurements of benthic foraminifera, fossil corals) (Dickson, 2002; Horita et al., 2002; Coggon, 2010; Rausch et al., 2013; Brennan et al., 2013;Gothmann et al., 2015; Evans et al., 2018). The modern day seawater Mg/Ca value is 5.2 mol/mol (Broecker & Peng, 1982) and Miocene estimates derived from proxy data show an increase from 30 Ma to modern day. Several studies have used modelling to explore variations in Mg/Ca_{sw} with predictions for Mg/Ca_{sw} derived from pore water modelling data for the past 20 Myr (Fantle & DePaolo, 2006; hereafter FD06) and 40 Myr (Higgins & Schrag, 2012; hereafter HS12). Given the residence time of Mg and Ca, these models exhibit potentially short-term changes in Mg/Ca_{sw} and further predicts a large and rapid increase in Mg/Ca seawater over the Neogene, with considerable uncertainty in the input parameters (Figure S3). The estimated SSTs for ODP Site 761 show a large divergence particularly between the HS12 SST scenarios and others, with SST >35 °C in the MCO. Overall, we prefer the proxy data compilation as it derived from range of disparate proxies which converge to show a consistent increase in Mg/Ca_{sw} (Figure S4). Note we do not include the fossil coral data from Gothmann et al., (2015) data as it contains a considerable amount of variability. Thus, to account for changes in Mg/Ca_{sw} we fit a 4^{th} order polynomial curve fit (eq. 3) through compiled Mg/Ca_{sw} proxy records to account for the changes in Cenozoic Mg/Ca_{sw} (eq. 3; Figure S5) including those derived from calcite veins (Coggon et al., 2010; Rausch et al., 2013), fluid inclusions (Horita et al., 2002; Brennan et al., 2013), echinoderms (Dickson et al., 2002), and larger benthic foraminifera (Evans et al., 2018).

$$seawater\ \frac{Mg}{Ca} = 5.3 - (0.153 * Age) + (0.00257 * Age^2) - (1.88e^{-5} * Age^3) + (4.85e^{-8} * Age^4) \quad \text{(eq. 3)}$$

In addition to variations in seawater Mg/Ca, when converting planktic Mg/Ca into temperature there must be consideration of non-thermal influences on shell Mg/Ca such as changes in salinity and the carbonate system. Studies have shown a positive relationship between salinity and shell Mg/Ca for some species *(G. ruber, O. universa, T. sacculifer*) with a sensitivity of ~4 to 5% per PSU (Kisakurek et al., 2008; Duenas-Bohorquez et al., 2009; Honisch et al., 2013). Further, Gray and Evans (2019) demonstrated that changes in pH influences shell Mg/Ca with a -7.3% per increase in 0.1 pH unit and proposed a multi-variable temperature calibration. However, their work shows that pH sensitivity is observed in some species (e.g., *O. universa, G. ruber,* and *G. bulloides*) and not others (e.g., *T. sacculifer*). Building on this carbonate system control, Holland et al., (2020) suggest that not pH but changes in dissolved inorganic carbon (DIC) drive variations in *O. universa* Mg/Ca, with an increase in DIC corresponding to an increase in Mg/Ca, however further work is needed to explore the possible DIC sensitivity across a range of species.

Here we present a new planktic record based on *D. altispira* Mg/Ca (near surface dweller, symbiont bearing) and revisit the Mg/Ca record derived from planktic *T. trilobus (*mixed layer dweller, symbiont bearing) previously published by Sosdian et al., (2020) (Figure S6; S7) across the middle Miocene. Available records of the carbonate system across the middle Miocene suggest changes in the surface ocean pH and carbon reservoir (Foster et al., 2012; Badger et al., 2013; Greenop et al., 2014; Sosdian et al., 2018; Sosdian et al., 2020) and we consider these below when estimating SST. There is limited information on salinity variations in the Indo-Pacific across the middle Miocene (Holbourn et al., 2010), but we conduct a sensitivity analysis to consider these possible changes.

We calculate paleotemperatures from both records with consideration of the factors described above. *D. altispira* is an extinct species and does not have a modern taxa equivalent. However, the *D. altispira* Mg/Ca variations are similar to those from other modern planktic taxa. For example, the range of Miocene Mg/Ca values (mean=3.6, max=3.9, min=3.3 mmol/mol) is similar to *G. ruber*, *T. trilobus*, and *G. bulloides* Mg/Ca values (mean=3.6, max=4.7, min=1.7 mmol/mol) (this study; Kuhnert et al., 2009; Tripati et al., 2009). Thus, to estimate the calcification temperature from *D. altispira* Mg/Ca, we assume that this species incorporates Mg into its calcite lattice similarly to modern taxa. However, across the middle Miocene, a boron isotope derived pH compilation shows an increase of 0.1 pH units (Fig. 2A) (Sosdian et al., 2018). As *D. altispira* is an extant species, accounting for changes in the carbon system and its influences is not straightforward, as some modern species are insensitive to pH changes (Gray & Evans, 2019). Here we apply the multi-species Mg/Ca-pH

correction from Evans et al., (2016) to assess the impact of middle Miocene pH increase on Mg/Ca ratios and the SST reconstruction

$$Mg/Ca_{CORRECTED} = (1 - (8.05 - pH) \times 0.70 \pm 0.18) \times Mg/Ca_{MEASURED.} \quad \text{(eq. 4)}$$

For pH we use the interpolated pH estimates from Sosdian et al., (2018). Briefly, a smoothed trendline was fitted through the 'G17' pH scenario and interpolated at the sampling resolution of the *D. altispira* Mg/Ca dataset.

Due to the lack of site specific records documenting salinity variations across the middle Miocene, we perform a sensitivity analysis assuming modern, +1 PSU above modern, and -1 PSU below modern. We apply the multi-species Mg/Ca-salinity correction from Hollis et al., (2019) to explore the impact of middle Miocene salinity changes.

$$Mg/Ca_{CORRECTED} = (1 - (salinity - 35) \times 0.042 \pm 0.008) \times Mg/Ca_{MEASURED} \quad \text{(eq. 5)}$$

We convert *D. altispira* Mg/Ca to SST using the multi-species equation of Anand et al., (2003) which has an exponential constant A=0.09 and pre-exponential constant B=0.38. The temperature equation is as follows:

$$\frac{Mg}{Ca}_{foram} = \frac{\frac{Mg}{Ca}_{sw}(t)}{\frac{Mg}{Ca}_{sw}(0)}^{0.41} \; 0.38e^{0.09T} \qquad \text{(eq. 6)}$$

Where Miocene Mg/Ca_{sw} (t) is estimated using eq. 3 (this study). In previous studies, a linear relationship between Mg/Ca_{foram} and Mg/Ca_{sw} was assumed (Lear et al., 2000). However it has since been shown that a power function best describes this relationship (Hasiuk & Lohmann, 2010; Lear et al., 2015). Here we use the power law constant of C=0.41, similar to the value applied for *T. trilobus*, a symbiont-bearing, mixed layer dweller (Delaney et al., 1985; Evans and Müller 2012).

Converting *T. trilobus* Mg/Ca ratios in SSTs is more straightforward, as thermal and non-thermal influences on *T. sacculifer* Mg/Ca are better constrained. Gray and Evans (2019) showed that *T. sacculifer* Mg/Ca is insensitive to pH change but sensitive to salinity changes. Previously, mean annual SSTs were calculated for *T. trilobus* in Sosdian et al., (2020), using the *T. sacculifer* calibration without sac from Anand et al., (2003) where A=0.09, B=0.347 after accounting for seawater Mg/Ca assuming a power constant of C= 0.41 as determined by

373 Evans and Müller (2012) based on the data of Delaney et al., (1985). Those authors assumed
374 a constant value of 3.43 mol/mol for seawater Mg/Ca derived from fluid inclusion data
375 (Horita et al., 2002) for the duration of the record. Here we modify the approach of Sosdian
376 et al., (2020) to incorporate varying seawater Mg/Ca as set out in this study for $\frac{Mg}{Ca}_{sw}(t)$ term
377 in the paleotemperature calculation (eq. 3; Figure S5; Fig. 2B). Further we consider it more
378 appropriate to use the species-specific equation of Gray and Evans (2019) which takes into
379 account changes in temperature and salinity to estimate SST (eq.7).
380
381 Mg/Ca = exp(a(S-35) + bT + c(pH-8) + d). (eq. 7)
382
383 Where a=0.054, b=0.063, c=0.01, and d=-0.24. Due to the lack of site specific records
384 documenting salinity variations across the middle Miocene in the Indian Ocean, we perform a
385 sensitivity analysis assuming modern, +1 PSU above modern, and -1 PSU below modern
386 salinity, similar to the analysis for ODP site 806.
387
388 To compare these tropical SST records to the high latitudes, we include the orbitally resolved
389 Southern Ocean *G. bulloides* Mg/Ca record from ODP Site 1171 (Shevenell et al., 2004).
390 Shevenell et al., (2004) converted G. *bulloides* Mg/Ca to SST using the Mg/Ca-SST
391 temperature equation from Mashiotta et al., (1999) and assumed modern Mg/Ca_{sw}. Here, to
392 ensure consistency amongst the comparisons, we recalculate SST from this Mg/Ca record
393 using the Gray and Evans (2019) multi-variable regression (eq. 7) for *G. bulloides* Mg/Ca,
394 where a=0.036, b=0.064, c=-0.88, and d=0.15 which takes into account temperature, pH, and
395 salinity. We use the interpolated pH record (Figure 2A) and the polynomial regression (eq. 3)
396 to estimate Mg/Ca seawater variations through the interval, and a C value of 0.72 (eq. 2) based
397 on calibration data (Evans et al., 2016). Due to the lack of site specific records documenting
398 salinity variations across the middle Miocene in the Southern Ocean, we perform a sensitivity
399 analysis assuming modern (34.5), +1 PSU above modern, and -1 PSU below modern salinity,
400 similar to ODP Sites 806 and 761.
401 In section 3.1 we present the planktic Mg/Ca records from ODP Sites 806 and 761 across the
402 middle Miocene and highlight the main their main features. In section 3.2 we consider the
403 thermal and non-thermal influences on these records and implications for interpretation and
404 uncertainties associated with the SST and planktic oxygen isotope records and paleoclimatic
405 variations.
406

2.6 Foraminiferal Preservation

Diagenesis alters the elemental composition of the test via partial dissolution, overgrowths, or recrystallization, and thus burial conditions and preservation of the calcite test need to be considered (Edgar et al., 2015). Partial dissolution in the water column or at the seafloor selectively removes Mg^{2+} from the foraminiferal test (Rosenthal and Lohmann, 2002; Dekens et al., 2002; Regenberg et al., 2006). This dissolution effect is critical at carbonate saturation values below 20 μmol/kg, as defined from core-top studies. Calcite dissolution decreases Mg/Ca and increases $\delta^{18}O_p$, acting to bias both toward cooler values.

ODP Site 806 lies well above the modern lysocline and was above it during the middle Miocene. SEM images of *D. altispira* from ODP Site 806 show original microstructure with minimal infilling and dissolution indicators (Figure S2). However, although ODP Site 806 is above the lysocline, modern carbonate saturation (ΔCO_3^{2-}) values are on average 10 μmol/kg (data from WOCE cruise P10, station 10, Lewis and Wallace, 1998). Regenberg et al., (2006) showed that the critical threshold values for which Mg^{2+} loss initiates is 20 μmol/kg and thus ideally Mg/Ca values should be corrected for dissolution. However, the species-specific equation established from core-tops in the Regenberg et al., (2006) study and others (Dekens et al., 2002; Rosenthal and Lohmann 2002) is not applicable to *D. altispira* as it is an extinct species. Here we compare the Mg/Ca and $\delta^{18}O_p$ records with dissolution indicators to assess whether temporal changes in calcite preservation could affect the interpretation of paleoclimate records at ODP Site 806. Potential dissolution indicators, such as percent coarse fraction (%CF) and average shell weight do not covary with Mg/Ca or $\delta^{18}O_p$ (R^2<0.2; Figure S6). This suggests minor effects of dissolution on these records and moving forward we assume that the overall changes in Mg/Ca and $\delta^{18}O_p$ at ODP Site 806 are related to climatic signals.

Several lines of evidence suggest that dissolution does not significantly affect the $\delta^{18}O_p$ or Mg/Ca values at ODP Site 761 as well. ODP Site 761 is situated well above the modern lysocline, above the critical 20 μmol/kg ΔCO_3^{2-}, in a relatively shallow burial depth during the middle Miocene (<50 m). Visual examination (Figure S2) of *T. trilobus* from ODP Site 761 shows moderately good preservation with no visible signs of infilling or dissolution. Average shell weight of *T. trilobus*, from the 300-355 μm size fraction does not covary (R^2=0.20) with the $\delta^{18}O_p$ or Mg/Ca record, supporting our argument that these values are not biased (Figure S7).

Despite the reasonable appearance of foraminifera from both sites, all tests appear frosty or opaque in contrast to exceptionally well preserved translucent test shells from hemipelagic muds (Pearson et al., 2001). However, this preservation state is typical of most

deep-sea carbonates and is caused by micro-recrystallization of calcite. Diagenesis likely affected the absolute $\delta^{18}O_p$ values, however large scale textural changes caused by recrystallization are not evident in SEM images (Figure S2) suggesting that diagenesis did not drive prominent shifts in $\delta^{18}O_p$. Additionally, Sr/Ca ratios from both cores show relatively high values (~1.1-1.2 mmol/mol) that are consistent across much of the record suggesting that diagenesis did not have a major influence on the variations of Mg/Ca and $\delta^{18}O_p$. Furthermore, Sexton et al., (2006) showed that Mg/Ca values decrease by a negligible amount with initial diagenetic alteration, thus temporal changes in Mg/Ca are less likely to be affected. For the reasons outlined above we believe that diagenesis had a minimal effect on our records and we therefore interpret the geochemical records in terms of changing paleoceanographic conditions and interpret relative changes in SST rather than absolute SSTs.

2.7 Calculation of surface seawater $\delta^{18}O$

To assess changes in surface ocean evaporation and precipitation changes in the Indo-Pacific region we use combined measurements of $\delta^{18}O_p$ and Mg/Ca from surface dwelling foraminifera, *D. altispira* and *T. trilobus* (Fig. 2C; Figure S6, S7). The foraminiferal $\delta^{18}O_p$ signal is dependent upon SST, salinity, and ice volume, whereas the Mg/Ca signal is primarily a temperature signal. Here we calculate planktic $\delta^{18}O_{sw}$ using the following equation (8) from Bemis et al., (1998):

$$\delta^{18}O_{sw}(V-SMOW) = 0.27 + \frac{((T(°C)-16.5+4.8\times\delta^{18}O_C(V-PDB)}{4.8} \quad \text{(eq. 8)}$$

The calculated $\delta^{18}O_{sw}$ reflects a combination of changes in global ice volume and local changes in $\delta^{18}O_{sw}$ attributable to local salinity changes. We compare overall changes in $\delta^{18}O_{sw}$ at each site which approximates changes in salinity (Rohling et al., 2007). Calculation of absolute salinity requires assumptions regarding the relationship between $\delta^{18}O_{sw}$ and salinity at a regional level and how this relationship has changed in the past. Thus, due to the large uncertainties associated with this assumption we interpret the $\delta^{18}O_{sw}$ record in terms of salinity variations but do not calculate absolute salinity.

3. Results

3.1 Mg/Ca records from the middle Miocene

At ODP Sites 806 and 761, planktic Mg/Ca decreases across the MMCT (14-13 Ma) along with the positive increase in benthic foraminiferal $\delta^{18}O$ ($\delta^{18}O_b$) indicative of cooling and Antarctic glaciation (Fig. 2C). A point to point comparison shows that ODP Site 806 *D. altispira* Mg/Ca declines by 0.60 mmol/mol (i.e. 3.85 to 3.25 mmol/mol) and 761 *T. trilobatus* Mg/Ca declines by 0.90 mmol/mol (i.e. 4.6 to 3.5 mmol/mol) (Fig. 2C) from 14.0

to 13.0 Ma. Average Mg/Ca values in the warm MCO (16.5-15 Ma) were higher than post-MMCT (13-11.5 Ma) at both sites (Fig. 2C) with ODP Site 806 Mg/Ca values decreasing from 3.7 to 3.5 mmol/mol and ODP Site 761 Mg/Ca values decreasing from 4.1 to 3.8 mmol/mol, respectively. During the MCO, both Mg/Ca records show short-term variations with higher Mg/Ca ratios aligning with more negative $\delta^{18}O_b$ values or periods of warmth/reduced ice volume. Overall the similarities in planktic Mg/Ca and $\delta^{18}O_b$ suggest that Mg/Ca is reflecting temperature variations across the middle Miocene.

3.2 Sensitivity Analysis

As stated previously, to consider the potential impact of pH and salinity changes on the long-term trends in Mg/Ca, we perform a sensitivity analysis. Specifically, we consider the influence of (1) varying pH and salinity on *D. altispira* Mg/Ca-SST and $\delta^{18}O_{sw}$ estimates and (2) varying salinity on *T. trilobus* Mg/Ca-SST and $\delta^{18}O_{sw}$ estimates.

As specified in section 2.5, we employ a pH and salinity correction to *D. altispira* Mg/Ca ratios to examine the influence on the long and short-term trends in Mg/Ca (Fig. 3). The magnitude of uncertainty on the Mg/Ca temperatures due to unconstrained salinity variations is ±1°C (Fig. 3A). The pH-corrected and pH-uncorrected *D. altispira* Mg/Ca record shows similar values following the MMCT with a gradual increase in Mg/Ca. However, during the MCO the pH corrected and uncorrected Mg/Ca records diverge with the pH corrected Mg/Ca lower by ~0.3 mmol/mol equivalent to ~1°C (Fig. 3B). During the MCO, the pH corrected Mg/Ca record shows lower average Mg/Ca values relative to the post-MMCT time interval. However, both pH corrected and pH uncorrected Mg/Ca records show a cooling associated with the MMCT and similar short-term variations during the MCO (i.e. higher Mg/Ca values during the warm periods) (Fig. 3B).

As stated in section 2.5, some species, such as symbiont bearing *T. sacculifer* are insensitive to pH changes. In the same vein, it is therefore possible that *D. altispira*, a symbiont bearing species as well, might have a similarly muted response. Additionally, more work is needed to identify the controlling carbonate system parameter on foraminifera, given that some studies suggest pH or DIC. We also acknowledge that without a site specific pH reconstruction, it is difficult to determine if the boron isotope pH derived record from the Indian and Pacific Ocean is representative for the WPWP region. Considering these uncertainties and unknowns, here we employ the multi-species calibration from Anand et al., (2003) (eq. 6) to estimate SSTs in the WPWP. To account for the uncertainty associated with pH and salinity variations, we incorporate an uncertainity envelope of ±2°C from 16.5 to 13.0 Ma and ±1°C from the

13.0 to 11.5 Ma in the ODP Site 806 SST reconstruction and present an associated uncertainty enveloped in the corresponding $\delta^{18}O_{sw}$ reconstruction.

As specified section 2.5, to convert *T. trilobus* Mg/Ca into temperature, we apply the Gray and Evans (2019) temperature equation with variable seawater Mg/Ca estimates from this study. Sosdian et al., (2020) use a constant Miocene Mg/Ca_{sw} value of 3.43 mol/mol which is within the range of Miocene Mg/Ca_{sw} values (3.4-3.9 mol/mol) applied here. The recalculated SST record from *T. trilobus* Mg/Ca data presented in Sosdian et al., (2020) has lower absolute values in comparison to the Sosdian et al., (2020) estimates but similar short-term and long-term trends (Figure S8). We consider this a more appropriate approach as the polynomial regression used in this study includes compiled seawater Mg/Ca proxy records from a range of approaches.

We perform a sensitivity analysis to consider changes in salinity and its influence on the SST record. Figure 4 shows the three SST and $\delta^{18}O_{sw}$ reconstructions for the salinity sensitivity analysis. The magnitude of uncertainty on the Mg/Ca temperatures due to unconstrained salinity variations is ±1°C. To account for the salinity uncertainty we incorporate an uncertainity envelope of ±1°C in the ODP Site 761 SST reconstruction and present an associated uncertainty enveloped in the $\delta^{18}O_{sw}$ reconstruction.

Here we also revisited the *G. bulloides* Mg/Ca dataset from Shevenell et al., (2004). These authors used the Mashiotta et al., (1999) Mg/Ca-T equation and assumed modern Mg/Ca_{sw} to calculate SST. Here, we calculate SST in the similar manner to the *T. trilobus* record where we apply the Gray and Evans (2019) equation with variable Mg/Ca_{sw} (this study) and pH correction. We perform a salinity sensivity analysis in the similar vein as above. Figure S9 shows the SST reconstructions from the salinity sensitivity analysis. The magnitude of uncertainty on the Mg/Ca temperatures due to unconstrained salinity variations is ±0.5°C. As expected, the ODP 1171 recalculated Mg/Ca-SST record has higher absolute values, due to lower Mg/Ca_{sw} values used to to estimate SST. The overall short-term and long-term trends are similar to the original record (Shevenell et al., 2004; Figure S9). To account for the salinity uncertainty we incorporate an uncertainity envelope of ±0.5°C in the SST reconstruction.

In section 3.2 we present and review the main features of ODP Site 806 and revisited ODP

site 761 Mg/Ca-SST reconstructions with their corresponding uncertainty envelopes as specified above. Alongside this, we present the $\delta^{18}O_{sw}$ reconstructions with an uncertainty envelope as specified above. Overall when comparing the SST and $\delta^{18}O_{sw}$ trends, we present the relative anomaly, as relative change with respect to baseline average from 15.5-16.0 Ma, with uncertainty envelopes as specified above. This approachs helps avoid additional uncertainties on absolute values associated with the factors mentioned above (e.g. Mg/Ca_{sw}, diagenesis).

3.2 Mg/Ca-temperature and $\delta^{18}O$ history

The near-surface dwelling species *D. altispira* Mg/Ca temperature record of ODP Site 806 in the western equatorial Pacific broadly varies by 2°C between cold and warm periods. From 14.1 to 13.7 Ma, SSTs in the western equatorial Pacific sharply cooled by ~1.8°C coincident with Antarctic glaciation and the positive $\delta^{18}O_b$ excursion at ODP Site 806 (Figure 5A). However, following the MMCT the reconstructed SST record shows a gradual long-term warming of ~1°C from 13.5 to 11.5 Ma.

The *D. altispira* $\delta^{18}O_p$ data from this study compare well with the previously published *D. altispira* and *T. trilobus* $\delta^{18}O_p$ records from Corfield and Cartlidge (2003) and Nathan and Leckie (2009) and here we compile all these datasets (Figure 5B). Average *D. altispira* $\delta^{18}O_p$ decreases from the early MCO (-0.76‰) to the lowest values around ~ 15 Ma (-1.25‰), followed by a small increase following the MMCT (to -0.92‰). The compiled *D. altispira* $\delta^{18}O_p$ long-term trend does not bear resemblance to the Mg/Ca-SST record at this site indicating that the $\delta^{18}O_p$ signal largely reflects changes in surface ocean $\delta^{18}O_{sw}$. The *D. altispira* $\delta^{18}O_p$ record differs markedly from the $\delta^{18}O_b$ with no change across the climate transition itself, suggesting that variations in local salinity are compensating for the global increase in $\delta^{18}O_{sw}$ caused by the glaciation.

The surface dwelling *T. trilobus* Mg/Ca-SST record from eastern equatorial Indian Ocean ODP Site 761 shows small long-term 1.5°C cooling across the middle Miocene calculated by averaging the SST estimates from before and after 14.0-13.5 Ma. This small long-term cooling is punctuated by a sharp 2.8°C cooling from 14.0 to 13.8 Ma concomitant with the positive benthic $\delta^{18}O_b$ excursion from 14.1 to 13.9 Ma indicative of a sea level change associated with Antarctic glaciation (Holbourn et al., 2004; Lear et al., 2010; John et al., 2011) (Fig. 6). SSTs varied by ~3°C between warm, deglaciated and cool, glaciated conditions prior to the MMCT. Around 13.5 Ma following the sharp decrease in temperature and transition into the stable icehouse of today, SSTs varied by 2°C.

582 The middle Miocene long-term cooling and decrease in SST variability are not
583 reflected in the corresponding $\delta^{18}O_p$ record (Fig. 6). Average $\delta^{18}O_p$ decreases from the early
584 MCO (-0.45 ‰) to the late middle Miocene (-0.87 ‰). $\delta^{18}O_p$ values show a sharp positive
585 excursion of 0.86 ‰ synchronous with the SST cooling and $\delta^{18}O_b$ excursion from 14.1-13.9
586 Ma followed by a return to average pre-excursion values. The $\delta^{18}O_p$ (Fig. 6B) record shows a
587 long-term decrease at this site indicative of a possible freshening and fluctuates considerably
588 across the middle Miocene implying that substantial variations in salinity are superimposed
589 on the $\delta^{18}O_p$ curve.
590 Using the Mg/Ca-derived SST records from ODP Sites 806 and 761 we reconstruct
591 variations in $\delta^{18}O_{sw}$ at both sites (Figure 7B). ODP Site 806 $\delta^{18}O_{sw}$ shows short-term
592 variability during cold and warm periods prior to the MMCT with no discernible change in
593 $\delta^{18}O_{sw}$ across the middle Miocene or the MMCT. In agreement with ODP Site 806, ODP Site
594 761 shows similar short term changes across the middle Miocene but of larger magnitude
595 with variations ~1 ‰ pre-MMCT, with fresher conditions during cooler, icier intervals and
596 saltier conditions during warmer, less icy intervals. In contrast to the indiscernible long-term
597 change at ODP Site 806, the ODP Site 761 $\delta^{18}O_{sw}$ record shows a long-term freshening trend
598 from the warmth of the MCO to the post-MMCT conditions. This is punctuated by a sharp
599 freshening from 13.9-13.4 Ma following by small amplitude (~0.5 ‰) variability post-
600 MMCT. Overall these $\delta^{18}O_{sw}$ records indicate a dynamic hydrologic history of the Indo-
601 Pacific region and that the Indian Ocean freshened relative to the Pacific following the major
602 glaciation step at 13.9 Ma. Although we do caveat that due to the low resolution of the ODP
603 806 SST record and its associated uncertainties (pH, salinity correction), interpretation of the
604 806 $\delta^{18}O_{sw}$ record might evolve with a more detailed evaluation of salinity changes at this site
605 and the Mg/Ca-pH sensitivity for *D. altispira*.
606
607 **4. Discussion**
608 Our new trace metal and stable isotope records span a 5 Myr interval from the warmth of the
609 MCO through the MMCT (Fig. 5-7). Here we examine the overall features of the SST and
610 $\delta^{18}O_{sw}$ records across the middle Miocene on short and long-term (>1 Myr) time scales in
611 context of global changes in pCO_2 and ice volume to constrain the global nature of these
612 changes and any tropical-high latitude linkages. Further, we examine changes in
613 paleogeography and constriction of the Indonesian Seaway in driving regional surface
614 hydrography changes in the eastern tropical Indian Ocean.
615
616 **4.1. Tropical Sea Surface Cooling across the middle Miocene**

Previously, the magnitude and nature of temperature change deduced from low latitude isotopic records across the middle Miocene has been contentious (Stewart et al., 2004). Earlier isotopic studies of the tropical region suggested a warming in the Indo-Pacific region across the middle Miocene in contrast to our findings (Savin et al., 1985). Reconstruction of Miocene atmospheric CO_2 concentrations show higher than modern values of ~470-630 ppm from 17-15 Ma, with large swings in CO_2 concentrations during the MCO and a decline in CO_2 concentration across the MMCT of ~200 ppm (Foster et al., 2012; Badger et al., 2013; Greenop et al., 2014; Sosdian et al., 2018). These dynamic changes in CO_2 concentration occur alongside the waxing and waning of ice sheets and sea level (Figure 7; Lear et al., 2010; John et al., 2011). Under the high CO_2 concentrations of the MCO, climate models simulate a warmer-than-modern tropical Indo-Pacific region (Tong et al., 2009; Krapp & Jungclaus, 2011). Here we examine relative changes in Indo-Pacific SSTs, in lieu of examining absolute SSTs relative to modern, due to the uncertainties associated with estimating absolute SSTs in the middle Miocene.

During the MCO, the Indo-Pacific cooling and warming is tightly coupled to the waxing and waning of the ephemeral ice sheets and CO_2 (Figure 7). This is evident at 15.5 Ma where SSTs were warm during an interval of high pCO_2, high sea level stand, and warm deep ocean waters. At 15 Ma SSTs cool during an interval of low CO_2 concentrations, low sea level, and cool deep ocean waters (Shevenell et al., 2004; Lear et al., 2010; Foster et al., 2012; Sosdian et al., 2018). The orbitally resolved South China Sea SST record exhibits a SST pattern that generally follows this trend during the MCO (Holbourn et al., 2010) suggesting a tropics-wide response. During the MCO, temperature records in both the high and low latitudes are responding in a similar manner, evident from comparison of SST records from ODP Site 1171 and from this study (Fig. 8; Shevenell et al., 2004; Sosdian et al., 2020). Although correlation of age models is difficult due to differences in available stratigraphic datums at each site, from 16.8 to16.2 Ma both the high latitudes and tropics were warming together, evident when comparing similarly resolved SST records from ODP Sites 761 and 1171 (Fig. 8; Figure S10. S11). Overall, these oscillations in the Indo-Pacific region suggest that the tropics responded dynamically to changes in greenhouse gas forcing, alongside Antarctic ice sheet dynamics and high latitude temperature change.

Following the warmth of the MCO, atmospheric CO_2 concentrations declined with a punctuated CO_2 decrease associated with the glaciation event at 13.9 Ma (Foster et al., 2012; Badger et al., 2013; Sosdian et al., 2018). The 1.8-2.8°C cooling in the low latitude Indo-Pacific region is associated with the glaciation event and CO_2 decline at 13.9 Ma (Holbourn et al. 2004; Lear et al., 2010; Badger et al., 2013; Foster et al., 2012; Sosdian et al., 2018). A

low resolution alkenone-derived SST record from the eastern equatorial Pacific shows a 2 °C transient cooling around 14 Ma consistent with our findings and indicating a tropics wide response, although the reconstructed temperatures surrounding this transient cooling event are near the saturation limit of the proxy and the cooling may be a low end estimate (Rousselle et al., 2013). However, an orbitally resolved SST record from ODP Site 1146 in the SCS shows no long-term cooling across the MMCT but rather discrete warming events from 14.6 Ma onward associated with glaciation. These lines of evidence suggest that despite its tropical location the Indo-Pacific was not insensitive to temperature change across the middle Miocene. Further the tropics cooled in the EEP and Indo-Pacific region across the MMCT but distinct differences exist regionally in the tropical surface ocean across the Miocene.

Across the MMCT, the orbitally resolved Southern Ocean SST record shows three distinct cooling steps at 14.2, 14.0 and 13.9 Ma of a total magnitude of 6-7 ˚C (Figure 8; Figure S10) (Shevenell et al., 2004). This ODP Site 1171 SST record is of higher resolution (~9 kyr) across the MMCT interval (45 data points; 14.2 to 13.8 Ma) than ODP Site 761 (~37 kyr; 10 data points) and ODP Site 806 (~ 150 kyr; 3 data points) which makes a point to point comparison difficult. However, examination of the temperature trends at each site shows that the Indo-Pacific cooling step initiated at 14.0 Ma occurs synchronous with the final two steps in the Southern Ocean cooling (Figure 8).

This interpretation of the lead/lag nature of the SST records from the Indo-Pacific and Southern Ocean hinges on how tightly constrained site specific age models are, and whether the lead/lags could be within error of the age model across the middle Miocene. Overall, there are several reasons to support the interpretation of the lead of Southern Ocean cooling over the tropical Indian Ocean. The age model for ODP Site 1171 was developed based on 11 magneto- and five biostratigraphic (foraminifer) and seven stable isotope datums (Shevenell & Kennett, 2004) and has not been updated since original publication. The age model for ODP Site 761 is a fourth order polynomial fit based on the biostratigraphic and isotopic datums from Holbourn et al., (2004) and ODP Site 806 age model is based on fourth order polynomial fit through nannofossil and planktic foraminiferal biostratigraphical events (Lear et al., 2015). All biostratigraphic datums are on the on the Berggren et al., (1995) timescale. Within each record there are several datums that anchor the MMCT and further each site has a highly resolved $\delta^{18}O_b$ and $\delta^{13}C_b$ records that allow comparison to the individual SST records (Figure S10-S12; Table S1). The three step cooling as exhibited in the ODP Site 1171 Mg/Ca-SST record (14.2, 14.0, 13.9 Ma) precedes the positive $\delta^{18}O_b$ excursion (13.9 Ma), indicative of Antarctic ice growth by 0.30 Myr, whilst the cooling exhibited in the ODP Site

761 Mg/Ca-SST record (14.0 Ma) occurs in step with the positive $\delta^{18}O_b$ excursion (14.0 Ma) (Figure 8). Considering the lower resolution nature of the Mg/Ca-SST relative to the $\delta^{18}O_b$ record, the cooling at ODP Site 806 (13.97 Ma) occurs in step with the positive $\delta^{18}O_b$ excursion (13.91 Ma; Figure 8). In summary, the relative timing of the Mg/Ca-SST cooling compared with the $\delta^{18}O_b$ and $\delta^{13}C_b$ shifts are different at each site and suggest that the Southern Ocean cooling leads the Indo-Pacific by a few hundred thousand years (Figure 8).

The lead of Southern Ocean cooling versus ice volume has been tied to the decoupling of Southern Ocean surface hydrography and global ice volume, caused by circulation changes and/or thresholds for Antarctic ice growth (Shevenell et al., 2004). These new records support the global signature of the MMCT cooling from 14.0 to 13.9 Ma and hint that the early cooling in the Southern Ocean is tied to a regional change in climate and/or non-thermal influences on the ODP Site 1171 planktic Mg/Ca record. This indicates that both the high and low latitudes cooled as ice sheets advanced at 13.9 Ma supporting an important role for the carbon cycle in driving the glaciation (e.g., Foster et al., 2012) and/or representing important positive feedbacks (e.g., Badger et al., 2013).

Post-MMCT, ODP Site 806 shows a gradual overall warming of 1˚C from 13.5 to 11.5 Ma. However in contrast, following the MMCT, ODP Site 761 shows short term minor variations in SST but no long-term trend in SST from 13.5 to 11.5 Ma. SSTs from exceptionally well preserved foraminifera $\delta^{18}O_p$ records in Tanzania show a warming from 12.2 to 11.55 Ma, however this is based on only two time slices (Stewart et al., 2004). Available organic-based SST records from the middle late Miocene derive mostly from locations outside of the WPWP, due to the saturation of the proxy in SST greater than 29˚C. A $U^{k'}_{37}$-derived SST record the from EEP across the late middle Miocene shows no long-term change in SST (Rouselle et al., 2003) across the late middle Miocene. Other available $U^{k'}_{37}$-derived SST record only capture ~12.5 to 11.5 Ma and show no discernible long-term change in SSTs (Zhang et al., 2014; Herbert et al., 2016).

The gradual warming at ODP Site 806 could be driven by changes in CO_2 levels, however there is considerable uncertainty in CO_2 reconstructions during the late middle Miocene, with estimates showing either change or an increase from 13 Ma to 11 Ma (Bolton et al., 2016; Mejia et al., 2017; Sosdian et al., 2018). A paleogeographic modeling study shows that with a more open Indonesian Seaway the warm pool migrates west into the eastern Indian Ocean and closure acts to reduce the flow through the seaway and warm waters pile up on the eastern part of the seaway (von der Heydt & Dijkstra, 2011). Using $\delta^{18}O_p$ and foraminiferal

assemblage records (64 kyr resolution) from ODP Site 806, Nathan and Leckie (2009) showed there was a dynamic, deep thermocline in the western equatorial Pacific from 13.2 to 11.6 Ma with a stable warm pool forming after 11.6 Ma. Thus constriction of the Indonesian Seaway associated with eustatic sea level fall (59±6 m; John et al., 2011) across the MMCT could have altered the position of proto-warm pool and contributed to the gradual warming at ODP Site 806 until the formation of a stable warm pool. However, due to the low resolution nature of the ODP Site 806 SST record and uncertainty in the size and latitudinal extent of the late middle Miocene proto-warm pool, additional higher resolution record from the western equatorial Pacific are needed to fully resolve the evolution of the WPWP and its dynamics.

4.2 Tropical Indian Ocean surface freshening across the middle Miocene

Middle Miocene Antarctic cryosphere expansion had the potential to affect the tropical hydrological cycle and cause significant salinity changes (Chiang & Bitz, 2005). In this context, Holbourn et al., (2010) argued that records of South China Sea surface ocean hydrography are attributable to northward migration of the ITCZ induced by southern hemisphere glaciation events and subsequent favoring of the relatively warmer northern hemisphere following 14.5 Ma (Holbourn et al., 2010). Due to the low resolution of the $\delta^{18}O_{sw}$ from ODP Site 806 and uncertainty in non-thermal effects on Mg/Ca, we focus our discussion on the ODP Site 761 $\delta^{18}O_{sw}$. ODP Site 761 sits outside of the present-day ITCZ influence and thus the proposed northward shift of the ITCZ at 13.9 Ma would place the ITCZ even further north and does not explain the freshening at ODP Site 761 across MMCT. Here we consider the role of Antarctic glaciation and paleogeographic changes during the Miocene as a mechanism to explain the freshening in the tropical eastern Indian Ocean. Specifically, we propose that the freshening in the Indo-Pacific region was related to the constriction of the Indonesian Seaway passages, driven by Antarctic glaciation induced sea level fall and ongoing paleogeographic changes. We explore this mechanism further in Section 4.2.1, examining the influence the Indonesian Seaway has on the regional surface ocean hydrography in the Indo-Pacific Ocean.

4.2.1 Miocene Constriction of the Indonesian Seaway

The modern Indonesian Seaway, a critical tropical ocean passageway, transports heat and freshwater from the Pacific into the Indian Ocean (Gordon & Fine, 1996). The nature and type of flow through the Indonesian Seaway is dictated by the positions of deep basins and channels connecting the oceans, the dominant source water, and the openness of the seaway. The intensity and nature of these pathways is likely to have been affected by past changes in eustatic sea level on multiple time scales (Kuhnt et al., 2004). For example, during the Last

761 Glacial Maximum sea level was lower than today by ~120 m. Under these conditions, the
762 modern major deep flow through the Makassar Strait would have still persisted while the
763 shallow Timor Passage would have been exposed and flow reduced (Figure 9).
764
765 Plate reconstructions from Hall et al., (2002) show that SE Asia collided with Australia
766 around 25 Ma, restricting the deep water pathway between the Pacific and Indian Oceans. The
767 Makassar strait would have been wider than today and only shallow and intermediate waters
768 of possibly North Pacific origin would flow through, while shallow flow of water of South
769 Pacific origin possibly continued through Sulawesi and New Guinea. Kuhnt et al., (2004)
770 estimate that the Indonesian Seaway was at its narrowest from 10-5 Ma with no evidence for
771 tectonic changes between 17 and 12 Ma. Further, as stated previously, the openness of the
772 Indonesian Seaway is also key in setting the position of the WPWP and intensity of tropical
773 surface ocean circulation (von der Heydt & Dijkstra, 2011).
774
775 We propose that the eustatic sea level drop (59±6 m; John et al., 2011; Figure 7) at the
776 MMCT restricted the already relatively shallow Indonesian Seaway. The seaway constriction
777 would result in a change in the proportion of source waters transported through shallow
778 passages from primarily warmer, saltier South Pacific water to primarily colder, fresher North
779 Pacific water. The switch in source waters would act to cool and freshen the distal outflow
780 regions of the seaway and the Leeuwin Current, as evident in our ODP Site 761 SST and
781 $\delta^{18}O_{sw}$ records (Figure 7).
782 In addition to changes in the source waters, constriction of the Indonesian Seaway
783 might affect the intensity of the proto-Leeuwin Current. Presently, ODP Site 761 is under the
784 influence of the Leeuwin current, an anamolous eastern boundary current, transporting
785 tropical waters poleward along the west Australian coast. The Leeuwin current is primarily
786 fed from Indonesian seaway waters and to some extent remote equatorial Indian Ocean
787 waters and the flow is driven by large scale meridional pressure gradient (Wijffels et al.,
788 2002; Domingues et al., 2007)) (Fig.9). Thus, changes in the nature of the seaways that guide
789 the Indonesian waters from the Pacific to Indian Ocean, are of importance to the Leeuwin
790 Current. Indeed, paleoceanographic records on Cenozoic and Quaternary timescales suggest
791 that Leeuwin current intensity and composition was dictated by changes in source water and
792 Indonesian seaway connectivity (McGowran et al., 1997; Wyrwool et al., 2009; Spooner et
793 al., 2011).
794 Paleontological data along the northwestern shelf of Australia suggest the current
795 flowed episodically in the late Oligocene/earliest Miocene, but it is likely that the initiation of
796 the modern-day Leeuwin like current was established in the middle Miocene when the

tectonic structure was favorable (Wyrwoll et al., 2009). Here we postulate that the transport capacity of the Indonesian Seaway would have been restricted as the flow in the shallow passageways would have been minimized and the proto-Leeuwin current reduced. Reduced intrusion of Leeuwin current waters into the Indian Ocean could act to freshen and cool this region through increased northward transport of the opposing current, similar to the West Australian Current. Further, a reduction in Leeuwin Current would enhance coastal upwelling and enhance productivity (Veeh et al., 2000). Planktic to benthic carbon isotopic differences at ODP Site 761, an indicator of productivity, show that following the MMCT this region became more productive (Figure S13) in line with a reduction in the Leeuwin Current. Overall, these findings indicate a significant role for the Indonesian Seaway in development of modern surface ocean circulation in the Tropical Indian Oceans and tropical heat and moisture transport in these regions.

5. Summary and Conclusions

Here we present middle Miocene climate records derived from Mg/Ca and oxygen isotopes in planktic foraminifera from the eastern equatorial Indian Ocean and western equatorial Pacific Ocean. Our records show dynamic changes in SST across the middle Miocene with warmer SSTs during the Miocene Climatic Optimum and an abrupt cooling associated with the glaciation step at 13.9 Ma. It appears that the high latitudes cooled first, followed by Antarctic glaciation and concomitant cooling at both high and low latitudes. This finding supports a role for the carbon cycle in driving the glaciation and/or representing important positive feedbacks.

The Middle Miocene Climate Transition was associated with a significant freshening of the tropical eastern Indian Ocean relative to the western Pacific Ocean. We speculate that the sea level fall associated with the Antarctic ice sheet expansion constricted the Indonesian Seaway acting to modify the surface ocean circulation and hydrography in the Indo-Pacific region. More detailed records documenting the SST patterns in Pacific are needed to further explore the response and development of the modern western equatorial Pacific Ocean climate setting, and formation of the western Pacific Warm Pool. Nevertheless, it seems that the Middle Miocene Climate Transition represented a key phase of the evolution of tropical climate dynamics.

6. Acknowledgements

This research used samples and/or data provided by the International Ocean Discovery Program (IODP). Funding for this research was provided by NERC Grant NE/I006427/1 to CHL. We thank D. Lunt and A. Farnsworth for discussions on the climate implications of this study, P. Moffa Sanchez for constructive criticism on an earlier version of this manuscript, P. Pearson for assistance with foraminiferal taxonomy, and Anabel Morte-Rodenas for lab

assistance. All data presented in this study are given in the Supplementary Tables and deposited in the Zenodo online data repository DOI:10.5281/zenodo.4155835.

7. References

Ali, J. R., S. J. Roberts, and S. J. Hall (1994) The closure of the Indo-Pacific Gateway: a new plate tectonic perspective, in Proceedings of the international workshop on Neogene evolution of Pacific Ocean gateways, edited by F. Hehuwat, E. Utomo, and A. Dharma, pp. 10–20, Nishimura, Kyoto.

Anand, P., H. Elderfield, and M. H. Conte (2003), Calibration of Mg/Ca thermometry in planktonic foraminifera from a sediment trap time series, *Paleoceanography*, *18*(2).

Badger, M.P.S., Lear, C.H., Pancost, R.D., Foster, G.L., Bailey, T.R., Leng, M.J., Abels, H.A., (2013). CO_2 drawdown following the middle Miocene expansion of the Antarctic Ice Sheet. *Paleoceanography* 28.

Barker, S., M. Greaves, and H. Elderfield (2003), A study of cleaning procedures used for foraminiferal Mg/Ca paleothermometry, *Geochemistry Geophysics Geosystems*, *4*.

Bemis, B. E., H. J. Spero, J. Bijma, and D. W. Lea (1998), Reevaluation of the oxygen isotopic composition of planktonic foraminifera: Experimental results and revised paleotemperature equations, *Paleoceanography*, *13*(2), 150-160.

Berggren, W.A., Kent, D.V., Swisher, C.C., Aubry, M.P., (1995) A revised Cenozoic geochronology and chronostratigraphy. In: Berggren, W.A., Kent, D.V., Aubry, M.P., Hardenbol, J. (Eds.), Geochronology Time Scales and Stratigraphic Correlation: Framework for an Historical Geology. *SEPM Special Publication*, v. 54, pp.129-212.

Bialik, O. M., M. Frank, C. Betzler, R. Zammit, and N.D. Waldmann (2019) Two-step closure of the Miocene Indian Ocean gateway to the Mediterranean, *Scientific Reports,* 9, 8842, doi:10.1038/s41598-019-45308-7

Bolton, C.T., Hernandez-Sanchez, M.T., Fuertes, M.A., Gonzalez-Lemos, S., Abrevaya, L., Mendez-Vicente, A., Flores, J.A., Probert, I., Giosan, L., Johnson, J., Stoll, H.M., (2016). Decrease in coccolithophore calcification and CO_2 since the middle Miocene. *Nat. Commun.*7, 13.

Brennan, S.T., Lowenstein, T.K., Cendon, D.I. (2013). The major ion composition of Cenozoic seawater: the past 36 million years from fluid inclusions in marine halite. *American Journal of Science* 313, 713-775.

Broecker, W. S., and T.-H. Peng (1982), Tracers in the Sea, Eldigo, Palisades, New York.

Chaisson, W.P., Leckie, R.M. (1993). High-resolution Neogene planktonic foraminifer biostratigraphy of Site 806, Ontong Java Plateau (western equatorial Pacific). In: Berger, W.H., Kroenke, L.W., Mayer, L.A. (Eds.), Proceedings of the Ocean Drilling Program. *Scientific Results*, vol.130. Ocean Drilling Program, College Station, TX, pp. 137–178.

Chiang, J., Bitz, C.M., (2005) Influence of high latitude ice cover on the marine ITCZ, *Climate Dynamics*, 25, p477-496

Cleroux, C., E. Cortijo, P. Anand, L. Labeyrie, F. Bassinot, N. Caillon, and J.-C. Duplessy (2008), Mg/Ca and Sr/Ca ratios in planktonic foraminifera: Proxies for upper water column temperature reconstruction, *Paleoceanography*, *23*(3).

884 Coggon, R. M., D. A. H. Teagle, C. E. Smith-Duque, J. C. Alt, and M. J. Cooper (2010),
885 Reconstructing past seawater Mg/Ca and Sr/Ca from mid-ocean ridge flank calcium carbonate veins,
886 *Science*, 327, 1114–1117, doi:10.1126/science.1182252.

887 Corfield, R. M., and J. E. Cartlidge (1993), Oxygen and carbon isotope stratigraphy of the middle
888 Miocene, Holes 805B and 806B, in *Proc. ODP*, Sci. Results, vol. **130**, edited by W. H. Berger, L.
889 W. Kroenke, and L. A. Mayer, pp 307– 322, Ocean Drilling Program, College Station, Tex.,
890 doi:10.2973/odp.proc.sr.130.026.1993.

891 Dekens, P. S., D. W. Lea, D. K. Pak, and H. J. Spero (2002), Core top calibration of Mg/Ca in tropical
892 foraminifera: Refining paleotemperature estimation, *Geochemistry Geophysics Geosystems*, *3*.
893
894 Delaney, M. L., A. W. H. Be, and E. A. Boyle (1985), Li, Sr, Mg, and Na in foraminiferal calcite shelss
895 from laboratory culture sediment traps, and sediment cores, *Geochim. Cosmochim. Acta*, *49*(6), 1327-
896 1341.

897 Dickson, J. A. D. (2002), Fossil echinoderms as monitor of the Mg/Ca ratio of Phanerozoic Oceans,
898 *Scienc*e, 298, 1222–1224.

899 Domingues, C. M., M. E. Maltrud, S. E. Wijffels, J. A. Church, and M. Tomczak (2007), Simulated Lagrangian
900 pathways between the Leeuwin Current System and the upper-ocean circulation of the southeast Indian Ocean,
901 *Deep-Sea Research Part Ii-Topical Studies in Oceanography*, *54*(8-10), 797-817.

902 Dueñas-Bohórquez, A., R. E. Da Rocha, A. Kuroyanagi, L. J. De Nooijer, J. Bijma, and G. J. Reichart
903 (2011), Interindividual variability and ontogenetic effects on Mg and Sr incorporation in the
904 planktonic foraminifer Globigerinoides sacculifer, *Geochim. Cosmochim. Acta,* 75(2), 520–532,
905 doi:10.1016/j.gca.2010.10.006.

906 Edgar, K.M., Anagnostou, E., Pearson, P.N., Foster, G.L., (2015) Assessing the impact of diagenesis
907 on delta B-11, delta C-13, delta O-18, Sr/Ca and B/Ca values in fossil planktic foraminiferal calcite.
908 *Geochim. Cosmochim. Acta* 166, 189-209.
909
910 Elderfield, H. & G. Ganssen (2000) Past temperature and $d^{18}O$ of surface ocean waters inferred from
911 foraminiferal Mg/Ca ratios, *Nature*, 405, p. 422.
912
913 Evans, D., and W. Müeller (2012), Deep time foraminifera Mg/Ca paleothermometry: Nonlinear correction for
914 secular change in seawater Mg/Ca, *Paleoceanography*, *27*.
915
916 Evans, D., B. S. Wade, M. Henehan, J. Erez, and W. Müeller (2016), Revisiting carbonate chemistry
917 controls on planktic foraminifera Mg/Ca: implications for sea surface temperature and hydrology shifts
918 over the Paleocene Eocene Thermal Maximum and Eocene Oligocene transition, *Climate of the*
919 *Past*, *12*(4), 819-835.
920
921 Evans, D., Sagoo, N., Renema, W., Cotton, L. J., Müller, W., Todd, J. A., et al. (2018). Eocene
922 greenhouse climate revealed by coupled clumped isotope-Mg/Ca thermometry. *P. Natl. Acad. Sci,*
923 *115*(6), 1174-1179. Article.
924 http://doi.org/10.1073/pnas.1714744115
925
926 Fantle, M. S. and DePaolo, D. J. (2006) Sr isotopes and pore fluid chemistry in carbonate
927 sediment of the Ontong Java Plateau: Calcite recrystallization rates and evidence for a
928 rapid rise in seawater Mg over the last 10 million years. *Geochim. Cosmochim. Acta*
929 70, 3883-3904.
930
931 Foster, G. L., C. H. Lear, and J. W. B. Rae (2012), The evolution of pCO_2, ice volume and climate during the
932 middle Miocene, *Earth and Planetary Science Letters*, *341*, 243-254.
933
934 Fraile, I., S. Mulitza, and M. Schulz (2009), Modeling planktonic foraminiferal seasonality: Implications for
935 sea-surface temperature reconstructions, *Marine Micropaleontology*, *72*(1-2), 1-9.

Gallagher, S. J., M. W. Wallace, C. L. Li, B. Kinna, J. T. Bye, K. Akimoto, and M. Torii (2009), Neogene history of the West Pacific Warm Pool, Kuroshio and Leeuwin currents, *Paleoceanography*, *24*.

Gasperi, J. T., and J. P. Kennett (1992), Isotopic evidence for depth stratification and paleoecology of Miocene Planktonic foraminifera-Western equatorial Pacific DSDP site 289, *Pacific Neogene: Environment, Evolution, and Events*, 117-147.

Gasperi, J. T., and J. P. Kennett (1993), Vertical thermal structure evolution of Miocene surface waters: Western equatorial Pacific DSDP Site 289, *Mar. Micropaleontol.*, **22**(3), 235– 254, doi:10.1016/0377-8398(93)90046-Z.

Gordon, A. L., and R. A. Fine (1996), Pathways of water between the Pacific and Indian oceans in the Indonesian seas, *Nature*, 379 (6561), 146-149.

Gothmann A. M., Stolarski J., Adkins J. F., Schoene B., Dennis K. J., Schrag D. P., Mazur M. and Bender M. L. (2015) Fossil corals as an archive of secular variations in seawater chemistry since the Mesozoic. *Geochim. Cosmochim. Acta* 160, 188–208. https://doi.org/10.1016/j.gca.2015.03.018.

Gourlan, AT, L. M. Meynadier, C. J. Allègre (2008): Tectonically driven changes in the Indian Ocean circulation over the last 25 Ma: Neodymium isotope evidence. *Earth and Planetary Science Letters*, 267(1-2), 353-364,

Greenop, R., Foster, G.L., Wilson, P.A., Lear, C.H. (2014) Middle Miocene climate instability associated with high-amplitude CO2 variability. *Paleoceanography* 29, 845-853.

Gray, W. R., and D. Evans (2019), Nonthermal Influences on Mg/Ca in Planktonic Foraminifera: A Review of Culture Studies and Application to the Last Glacial Maximum, *Paleoceanography and Paleoclimatology*, *34*(3), 306-315.

Hall, R., Reconstructing Cenozoic SE Asia, In Tectonic evolution of Southeast Asia, edited by R. Hall and D. Blundell, *Geol. Soc. Spec. Pub*., 106, 153–184, 1996.

Hall, R., (2002) Cenozoic geological and plate tectonic evolution of SE Asia and the SW Pacific: computer-based reconstructions, model and animations, J. *Asian Earth Sci*., 20, 353–43.

Hamon, N., Sepulchre, P., Lefebvre, V., and Ramstein, G. (2013) The role of eastern Tethys seaway closure in the Middle Miocene Climatic Transition (ca. 14 Ma), *Clim. Past,* 9, 2687–2702, https://doi.org/10.5194/cp-9-2687-2013.

Hartman, J. D., Sangiorgi, F., Salabarnada, A., Peterse, F., Houben, A. J. P., Schouten, S., Brinkhuis, H., Escutia, C., and Bijl, P. K. (2018) Paleoceanography and ice sheet variability offshore Wilkes Land, Antarctica – Part 3: Insights from Oligocene–Miocene TEX_{86}-based sea surface temperature reconstructions, *Clim. Past*, 14, 1275–1297, https://doi.org/10.5194/cp-14-1275-2018, 2018.

Hasiuk, F. J., and K. C. Lohmann (2010), Application of calcite Mg partitioning functions to the reconstruction of paleocean Mg/Ca, *Geochim. Cosmochim. Acta, 74*(23), 6751-6763.

Herbert, T. D., Lawrence, K. T., Tzanova, A., Peterson, L. C., Caballero-Gill, R., & Kelly, C. S. (2016). Late Miocene global cooling and the rise of modern ecosystems. *Nature Geoscience*. https://doi.org/10.1038/ngeo2813

Higgins, J. and Schrag, D. (2012), Records of Neogene seawater chemistry and diagenesis in deep-sea carbonate sediments and pore fluids. *Earth Planet. Sci. Lett.* 357, 386-396 (2012).

Holbourn, A., W. Kuhnt, J. A. Simo, and Q. Y. Li (2004), Middle miocene isotope stratigraphy and paleoceanographic evolution of the northwest and southwest Australian margins (Wombat Plateau and Great Australian Bight), *Palaeogeography Palaeoclimatology Palaeoecology*, *208*(1-2), 1-22.

Holbourn, A., W. Kuhnt, M. Regenberg, M. Schulz, A. Mix, and N. Andersen (2010), Does Antarctic glaciation force migration of the tropical rain belt?, *Geology*, *38*(9), 783-786.

Holbourn, A., Kuhnt, W., Frank, M., Haley, B.A. (2013), Changes in Pacific Ocean circulation following the Miocene onset of permanent Antarctic ice cover. *Earth and Planetary Science Letters* 365, 38-50.

Holbourn, A.E., Kuhnt, W., Lyle, M.W., Schneider, L., Romero, O., and Andersen, N. (2014), Middle Miocene climate cooling linked to intensification of eastern equatorial Pacific upwelling: *Geology*, v. 42, p. 19–22, doi:10.1130/G34890.1.

Holland, K., Branson, O., Haynes, L., Honisch, B., Allen, K.A., Russell, A.D. et al. (2020), Constraining multiple controls on planktic foraminifera Mg/Ca, *Geochim. Cosmochim. Acta.*, v. 273, 116-136, https://doi.org/10.1016/j.gca.2020.01.015.

Hollis, C. J., et al. (2019), The DeepMIP contribution to PMIP4: methodologies for selection, compilation and analysis of latest Paleocene and early Eocene climate proxy data, incorporating version 0.1 of the DeepMIP database, *Geoscientific Model Development*, *12*(7), 3149-3206.

Hönisch, B., Allen, K.A., Lea, D.W., Spero, H.J., Eggins, S.M., Arbuszewski, J., deMenocal, P., Rosenthal, Y., Russell, A.D., Elderfield, H. (2013). The influence of salinity on Mg/Ca in planktic foraminifers - Evidence from cultures, core-top sediments and complementary delta O-18. *Geochim. Cosmochim. Acta,* 121, 196-213

Horita, J., H. Zimmermann, and H. D. Holland (2002), Chemical evolution of seawater during the Phanerozoic: Implications from the record of marine evaporites, *Geochim. Cosmochim. Acta*, *66*(21), 3733-3756.

John, C. M., G. D. Karner, E. Browning, R. M. Leckie, Z. Mateo, B. Carson, and C. Lowery (2011), Timing and magnitude of Miocene eustasy derived from the mixed siliciclastic-carbonate stratigraphic record of the northeastern Australian margin, *Earth and Planetary Science Letters*, *304*(3-4), 455-467.

Kennett, J.P., and Srinivasan, M.S. (1983) *Neogene Planktonic Foraminifera: A Phylogenetic Atlas:* Stroudsburg, PA: Hutchinson Ross.

Kennett, J. P., G. Keller, and M. S. Srinivasan (1985) Miocene planktonic foraminiferal biogeography and paleoceanography development of the Indo-Pacific region, *Geological Society of America Memoirs*, *163*, 197-236.

Key, R.M., Kozyr, A., Sabine, C.L., Lee, K., Wanninkhof, R., Bullister, J.L., Feely, R.A., Millero, F.J., Mordy, C., Peng, T.H. (2004) A global ocean carbon climatology: Results from Global Data Analysis Project (GLODAP). *Global Biogeochemical Cycles* 18.

Kisakurek, B., A. Eisenhauer, F. Bohm, D. Garbe-Schonberg, and J. Erez (2008), Controls on shell Mg/Ca and Sr/Ca in cultured planktonic foraminiferan, Globigerinoides ruber (white), *Earth and Planetary Science Letters*, *273*(3-4), 260-269.

Krapp, M. and Jungclaus, J. H. (2011) The Middle Miocene climate as modelled in an atmosphere-ocean-biosphere model, *Climates of the Past*, 7, 1169–1188, https://doi.org/10.5194/cp-7-1169-2011.

Kuhnert, H., T. Bickert, and H. Paulsen (2009), Southern Ocean frontal system changes precede Antarctic ice sheet growth during the middle Miocene, *Earth and Planetary Science Letters*, *284*(3-4), 630-638.

Kuhnt, W., A. Holbourn, R. Hall, M. Zuvela, and R. Kase (2004), Neogene history of the Indonesian throughflow, *Continent-Ocean Interactions within East Asian Marginal Seas*, *149*, 299-320.

Lear, C. H., H. Elderfield, and P. A. Wilson (2000), Cenozoic deep-sea temperatures and global ice volumes from Mg/Ca in benthic foraminiferal calcite, *Science*, *287*(5451), 269-272.

Lear, C. H., E. M. Mawbey, and Y. Rosenthal (2010), Cenozoic benthic foraminiferal Mg/Ca and Li/Ca records: Toward unlocking temperatures and saturation states, *Paleoceanography*, *25*.

Lear, CH., Coxall, HK., Foster, GL., Lunt, D., Mawbey, E. M., Rosenthal, Y., Wilson, P. A. (2015). Neogene ice volume and ocean temperatures: Insights from infaunal foraminiferal Mg/Ca paleothermometry. *Paleoceanography*, *30*, 1437-1454. https://doi.org/10.1002/2015PA002833

Levy, R., Harwood, D., Florindo, F., Sangiorgi, F., Tripati, R., et al. (2016) Antarctic ice sheet sensitivity to atmospheric CO_2 variations in the early to mid-Miocene, *P. Natl. Acad. Sci.* USA, 113, 3453–3458.

Lewis, A. R., D. R. Marchant, A. C. Ashworth, S. R. Hemming, and M. L. Machlus (2007), Major middle Miocene global climate change: Evidence from East Antarctica and the Transantarctic Mountains, *Geological Society of America Bulletin*, *119*(11-12), 1449-1461.

Lewis, E., and D. W. R. Wallace (1998), Program developed for CO_2 system calculations, *ORNL/CDIAC-105* , 21 pp., Carbon Dioxide Inf. Anal. Cent., Oak Ridge Natl. Lab., Oak Ridge, Tenn.

Mashiotta TA, Lea DW, Spero H.J. (1999), Glacial–interglacial changes in Subantarctic sea surface temperature and δ^{18}O-water using foraminiferal Mg, *Earth and Planetary Science Letters*, 170(4), 417-432.

Majewski, W. & S. M. Bohaty (2010), Surface-water cooling and salinity decrease during the Middle Miocene climate transition at Southern Ocean ODP Site 747 (Kerguelen Plateau), *Marine Micropaleontology*, *74*(1-2), 1-14.

McGowran, B., Q. Li, J. Cann, D. Padley, D.M.McKirdy, S. Shafik (1997) Biogeographic impact of the Leeuwin Current in southern Australia since the late middle Eocene, *Palaeogeogr. Palaeoclimatol. Palaeoecol.,* 136, pp. 19-40

Mejía, L.M., Mendez-Vicente, A., Abrevaya, L., Lawrence, K. T., Ladlow, C., Bolton, C. T., Cacho, I., Stoll, H.M. (2017): A diatom record of CO_2 decline since the late Miocene. *Earth and Planetary Science Letters*, 479, 18-33,

Nathan, S. A., and R. M. Leckie (2009), Early history of the Western Pacific Warm Pool during the middle to late Miocene (similar to 13.2-5.8 Ma): Role of sea-level change and implications for equatorial circulation, *Palaeogeogr. Palaeoclimatol. Palaeoecol.*, *274*(3-4), 140-159.

Norris, R. D., R. M. Corfield, and J. E. Cartlidge (1993), Evoluton of depth ecology in the planktic foraminifera lineage Globorotalia (Fohsella), *Geology*, *21*(11), 975-978.

Pattiaratchi, C. & M. Woo (2009) The mean state of the Leeuwin current system between North West Cape and Cape Leeuwin, *Journal of the Royal Society of Western Australia*, 92 (2), 221-241

Pearson, P.N. (1995). Planktonic foraminifer biostratigraphy and the development of pelagic caps on guyots in the Marshall Islands group. In: Haggerty, J.A., Premoli Silva, I., Rack, F., McNutt, M.K. (Eds.), Proc.

Pearson, P. N., Ditchfield, P.W., Singano, J., Harcourt-Brown, K., Nicholas, C.J. et al. (2001) Warm tropical sea surface temperatures in the Late Cretaceous and Eocene epochs. *Nature* 413(6855), pp. 481-487.

Rausch, S., Böhm, F., Bach, W., Klügel, A. & Eisenhauer, A. (2013) Calcium carbonate veins in ocean crust record a threefold increase of seawater Mg/Ca in the past 30 million years. *Earth and Planetary Science Letters.* 362, 215-224.

Regenberg, M., D. Nuernberg, S. Steph, J. Groeneveld, D. Garbe-Schoenberg, R. Tiedemann, and W.-C. Dullo

(2006), Assessing the effect of dissolution on planktonic foraminiferal Mg/Ca ratios: Evidence from Caribbean core tops, *Geochemistry Geophysics Geosystems*, *7*.

Regenberg, M., S. Steph, D. Nuernberg, R. Tiedemann, and D. Garbe-Schoenberg (2009), Calibrating Mg/Ca ratios of multiple planktonic foraminiferal species with delta O-18-calcification temperatures: Paleothermometry for the upper water column, *Earth and Planetary Science Letters*, *278*(3-4), 324-336.

Rohling, E. J. (2007), Progress in paleosalinity: Overview and presentation of a new approach, *Paleoceanography*, *22*(3).

Rosenthal, Y., and G. P. Lohmann (2002), Accurate estimation of sea surface temperatures using dissolution-corrected calibrations for Mg/Ca paleothermometry, *Paleoceanography*, *17*(3).

Rousselle, G., C. Beltran, M.-A. Sicre, I. Raffi, and M. De Rafelis (2013), Changes in sea-surface conditions in the Equatorial Pacific during the middle Miocene-Pliocene as inferred from coccolith geochemistry, *Earth and Planetary Science Letters*, *361*, 412-421.

Sangiorgi, F., Bijl, P. K., Passchier, S., Salzmann, U., Schouten, S., McKay, R., Cody, R. D., Pross, J., van de Flierdt, T., Bohaty, S. M., Levy, R., Williams, T., Escutia, C., and Brinkhuis, H. (2018) Southern Ocean warming and Wilkes Land ice sheet retreat during the mid-Miocene, *Nat. Commun*., 9, 317, https://doi.org/10.1038/s41467-017-02609-7.

Savin, S. M., L. Abel, E. Barrera, D. Hodell, J. P. Kennett, M. Murphy, G. Keller, J. Killingley, and E. Vincent (1985), The evolution of the Miocene surface and near-surface marine temperatures- oxygen isotopic evidence, *Geological Society of America Memoirs*, *163*, 49-&

Schlitzer, R. (2012) Ocean Data View. http://odv.awi .de.

Schneider, N. (1998) The Indonesian Throughflow and the global climate system, *J. Climate*, 11, 676–689.

Sclater, J. G., L. Meinke, A. Bennett, and C. Murphy (1985), The depth of the ocean through the Neogene, *Geological Society of America Memoirs*, *163*, https://doi.org/10.1130/MEM163-p1.

Scotese, C. R., L. M. Gahagan, and R. L. Larson (1988), Plate tectonic reconstructions of the Cretaceous and Cenozoic ocean basins, *Tectonophysics*, *155*(1-4), 27-48.

Sexton, P. F., P. A. Wilson, and P. N. Pearson (2006), Microstructural and geochemical perspectives on planktic foraminiferal preservation: "Glassy" versus "Frosty", *Geochemistry Geophysics Geosystems*, *7*.

Shevenell, A. E., J. P. Kennett, and D. W. Lea (2004), Middle Miocene Southern Ocean cooling and Antarctic cryosphere expansion, *Science*, *305*(5691), 1766-1770.

Shevenell, A.E., J. P. Kennett (2004), Paleoceanographic Change During the Middle Miocene Climate Revolution: An Antarctic Stable Isotope Perspective in The Cenozoic Southern Ocean: Tectonics, sedimentation, and climate change between Australia and Antarctica, N. F. Exon, J. P. Kennett, M. J. Malone, Eds. (American Geophysical Union, Washington D.C.)

Spooner, M. I., P. De Deckker, T. T. Barrows, and L. K. Fifield (2011), The behaviour of the Leeuwin Current offshore NW Australia during the last five glacial-interglacial cycles, *Global and Planetary Change*, *75*(3-4), 119-132.

Sprintall, J., Potemra, J. T., Hautala, S. L., Bray, N. A., and W. W. Pandoe (2003) Temperature and salinity variability in the exit passages of the Indonesian Throughflow. Deep Sea Res. II, 50, 2183–2204.

Sosdian, S. M., Greenop, R., Hain, M.P., Foster, G.L., Pearson, P.N., Lear, C.H. (2018) Constraining the evolution of Neogene ocean carbonate chemistry using the boron isotope pH proxy. *Earth and Planetary Science Letters* 498, 362-376, doi:10.1016/j.epsl.2018.06.017.

Sosdian, S.M., T. L. Babila, R. Greenop, G.L. Foster, and C.H. Lear (2020) Ocean carbon storage across the middle Miocene: a new interpretation for the Monterey Event, *Nat. Commun.* **11,** 134, https://doi.org/10.1038/s41467-019-13792-0

Spezzaferri, S., Kucera, M., Pearson, P.N., Wade, B.S., Rappo, S., Poole, C.R., Morard, R., Stalder, C. (2015) Fossil and Genetic Evidence for the Polyphyletic Nature of the Planktonic Foraminifera "Globigerinoides", and Description of the New Genus Trilobatus. *Plos One* 10.

Stewart, D.R.M., Pearon, P.N., Ditchfield, P.W., Singano, J.W. (2004),Miocene tropical Indian Ocean temperatures: evidence from three exceptionally preserved foraminiferal assemblages from Tanzania, *Journal of African Earth Sciences,* 40, p. 173-190.

Super, J. R., Thomas, E., Pagani, M., Huber, M., O'Brien, C., and Hull, P. M. (2018) North Atlantic temperature and pCO_2 coupling in the early-middle Miocene, *Geology*, 46, 519–522.

Tong, J.A.., You, Y., R.D. Müller, Seton, M. (2009) Climate model sensitivity to atmospheric CO_2 concentrations for the middle Miocene, *Global Planetary Change,* 67, p 129-140.

Tripati, A. K., Roberts, C. D., and Eagle, R. A. (2009) Coupling of CO_2 and ice sheet stability over major climate transitions of the last 20 million years, *Science,* 326, 1394–1397.

Veeh, H.H., McCorkle, D.C., Heggie, D.T. (2000) Glacial/interglacial variations of sedimentation on the West Australian continent margin: constraints from excess 230Th. Marine Geoloy. 166, 11–30.

Verducci, M., Foresi, L.M., Scott, G.H., Tiepolo, M., Sprovieri, M., and Lirer, F. (2007) East Antarctic Ice Sheet fluctuations during the Middle Miocene Climatic Transition inferred from faunal and biogeochemical data on planktonic foraminifera (Kerguelen Plateau). *U.S. Geological Survey and The National Academics;* USGS OF−2007−1047, Short Research Paper 037.

von der Heydt, A.S. & H.A. Dijkstra (2011) The impact of ocean gateways on ENSO variability in the Miocene. In :Hall, R; Cottam, M.A.; M.E.J. Wilson (eds.). The SE Asian Gateway: History of tectonics of the Australia-Asia Collision. *Geol. Soc. Spec. Pub.*, 355, 305-318.

Wajsowicz, R. C., and E. K. Schneider (2001) The Indonesian throughflow's effect on global climate determined from the COLA coupled climate system, *J. Climate,* 14, 3029–3042, 2001.

Wara et al. (2005) Permanent El Nino like conditions during the Pliocene warm period, Sciecne, v. 309, p. 758-761.

Wijffels, S., J. Sprintall, M. Fieux, and N. Bray (2002), The JADE and WOCE I10/IR6 throughflow sections in the southeast Indian Ocean. Part 1: water mass distribution and variability, *Deep-Sea Research Part Ii-Topical Studies in Oceanography*, *49*(7-8), 1341-1362.

Wyrwool, K.-H., Greenstein, B.J., Kendrick, G.W., Chen, G.S. (2009) The palaeoceanography of the Leeuwin Current: implications for a future world. Journal of the Royal Society of Western Australia, 92, 37-51.

Zachariasse, W-J (1992) Neogene planktonic foraminifers from sites 761 and 762 off *Northwest Australia.* In: von Rad, U; Haq, BU; et al. (eds.), Proceedings of the Ocean Drilling Program, Scientific Results, College Station, TX (Ocean Drilling Program), ***122****, 665-67.*

Zhang, Y. G., Pagani, M., & Liu, Z. (2014) A 12-Million-Year Temperature History of the Tropical Pacific Ocean. *Science, 344*(6179), 84-87. https://doi.org/10.1126/science.1246172

Figure Captions

Figure 1 Mean annual sea surface temperature (WOCE; Gouretski & Koltermann, 2004) showing modern locations of ODP sites used in this study (white triangles) and the location of the West Pacific Warm Pool (WPWP) and Indonesian Throughflow. The WPWP is the large body of water in the western Pacific denoted by SSTs greater than 28°C. Sea surface temperature plot made using Ocean Data View (Schlitzer, 2012).

Figure 2 Input parameters for Mg/Ca-temperature sensitivity analysis. (A) interpolated pH estimates derived from the '$\delta^{11}B_{sw}$-G17' reconstruction, fluid inclusion data for [Mg^{2+}] and [Ca^{2+}] seawater, and 'Pälike' CCD scenario (Sosdian et al., 2018); (B) Fourth order polynomial curve fit through compiled seawater Mg/Ca proxy records based on fluid inclusions, calcite veins, echinoderms, and large benthic foraminifera (Dickson, 2002, Horita et al., 2002, Brennan et al., 2013; Coggon et al., 2010; Rausch et al., 2013; Evans et al. 2018). The grey envelope represents the ±0.5 mol/mol uncertainty window. (C) Measured Mg/Ca ratios (mmol mol^{-1}) for *D. altispira* and *T. trilobus* from ODP Sites 806 and 761, respectively. Three scenarios for past changes in salinity at ODP Sites 806 and site 761 are explored, specifically assuming modern values for each site and ±1 PSU modern values.

Figure 3 ODP site 806 Mg/Ca sensitivity analysis output for a range of scenarios. ODP site 806 *D. altispira* Mg/Ca measured in comparison to Mg/Ca corrected for (A) salinity and (B) pH variations.

Figure 4 ODP site 761 Mg/Ca sensitivity analysis output for a range of scenarios. (A) SST estimates derived from ODP site 761 *T. trilobus* Mg/Ca with varying salinity scenarios (constant modern, constant modern +1 PSU, constant modern -1 PSU); (B) $\delta^{18}O_{sw}$ records using three salinity scenarios.

Figure 5 Climate proxy data from Ontong Java Plateau ODP Site 806 (0°19.1'N, 159°21.7'E). (A) Mg/Ca-SST anomaly from measured Mg/Ca (black circles) with uncertainty envelope specificed in text; (B) planktic foraminifera oxygen isotope records from this study and previously published records (Corfield & Cartlidge, 1993; Nathan & Leckie, 2009); (C) Benthic foraminifera oxygen isotope records from previously published records (Corfield & Cartlidge, 1993; Nathan & Leckie, 2009; Holbourn et al., 2013; Lear et al., 2015). MCO denotes the Miocene Climatic Optimum and MMCT denotes the middle Miocene Climate Transition and the timing is determined from the $\delta^{18}O_b$ record. Temperature anomaly was calculated as relative temperature change with respect to baseline average from 15.5-16.0 Ma.

Figure 6 Climate proxy data from Wombat Plateau ODP Site 761 (16°44.23'S, 115°32.10'E). (A) Mg/Ca-SST anomaly, generated on planktic foraminifera *T. trilobus* across the middle Miocene (Sosdian et al., 2020) with uncertainty envelope as specified in the text; (B) T. trilobus oxygen isotope record from this study; (C) Benthic oxygen isotope records from previously published records (Holbourn et al., 2004; Lear et al., 2010). MCO denotes the Miocene Climatic Optimum and MMCT denotes the middle Miocene Climate Transition and the timing is determined from the $\delta^{18}O_b$ record. Temperature anomaly was calculated as relative temperature change with respect to baseline average from 15.5-16.0 Ma.

Figure 7 Site comparison between ODP 806 and 761 (A) Temperature anomaly, as relative temperature change with respect to baseline average from 15.5-16.0 Ma, determined from planktic foraminifera Mg/Ca records from this study and Sosdian et al., (2020) with uncertainty envelope highlighted; (B) planktic $\delta^{18}O_p$ from *T. trilobus* (blue) and *D. altispira* (grey) from this study and previously published study (Corfield & Cartlidge, 1993);(C) $\delta^{18}O_{sw}$ anomaly, as relative $\delta^{18}O_{sw}$ change with respect to baseline average from 15.5-16.0 Ma and uncertainty envelope highlighted; (D) Boron isotope derived atmospheric pCO_2 record using three $\delta^{11}B_{sw}$ scenarios which incorporate various $\delta^{11}B_{sw}$ scenarios (LO2; RH13; G17), fluid inclusion Mg/Casw data, and 'Palike' CCD reconstructions (Sosdian et al., 2018). (E) Eustatic sea level change from the Marion Plateau (John et al., 2011 (F) Estimates of changes in global ice volume as derived from $\delta^{18}O_{sw}$ at ODP site 761. The shaded regions showcase the range in estimates between grey circles are uncorrected BWT estimates whereas dark grey circles are corrected for changes in deep ocean carbon saturation state changes (Lear et al., 2010). Note BWT estimates are corrected for changes in Mg/Ca_{sw}. MCO and MMCT denote the time intervals of the Miocene Climatic Optimum and the middle Miocene Climate Transition and the timing is determined from the $\delta^{18}O_b$ record. The 13.9 Ma glaciation step is highlighted by a purple vertical line. Uncertainty envelopes are included for ODP site 806 records and a uncertainty bar is used for ODP site 761 in panels A and C.

Figure 8 Comparison of Indo-Pacific ODP Sites 806 and 761 and Southern Ocean site 1171(A, B) Mg/Ca-derived SST anomaly for ODP site 806 and 761 (Sosdian et al., 2020; this study) and (C) Mg/Ca-derived SST anomaly from ODP site 1171 (Shevenell et al., 2004) recalculated in this study using the Gray and Evans (2019) multi-variable regression as specified in the text and variable Mg/Ca_{sw}. Uncertainty envelopes are plotted for each temperature reconstruction. (D, E) ODP Site 806 and 761 and (F) ODP Site 1171 benthic oxygen isotope records (Corfield & Cortlidge, 1993; Holbourn et al., 2004; Shevenell et al., 2004; Nathan & Leckie, 2009; Lear et al., 2010; Holbourn et al., 2013) from across the middle Miocene (13-15.5 Ma). The blue arrows highlights the cooling steps observed at each site. The temperature scale is different in panel A-B and C to showcase the variations in each location. The 13.9 Ma glaciation step is highlighted by a grey vertical line.

Figure 9 Modern regional surface ocean currents and study sites in the Indo-Pacific region. Indonesian throughflow straits include Makassar Strait, Lombok Strait, and Timor Passage. Surface ocean currents include North Equatorial Current (NEC), South Equatorial Current (SEC), North Equatorial Counter Current (NECC), Leeuwin Current (LC) and Western Australian Current (WAC). NP (North Pacific) and SP (South Pacific) sources waters are identified alongside of West Pacific Warm Pool (WPWP). Map made using Ocean Data View.

1296

Paleoceanography & Paleoclimatology

Supporting Information for

Initiation of the Western Pacific Warm Pool at the Middle Miocene Climate Transition?

S.M. Sosdian & C.L. Lear

[1]Cardiff University, School of Earth & Ocean Sciences, Cardiff, CF10 3AT, UK

Contents of this file

Introduction

We provide supporting information for our paleoclimate reconstructions associated with site-specific age models, study site locations, sample preservation, and SST sensitivity analysis. Specifically, we provide a map of mid-Miocene paleolocations for sites used in SST reconstructions. We present SEM images from the planktic foraminifera used in the trace metal and isotope records produced in this study and compare records of coarse fraction and average shell size from ODP site 806 and 761 alongside trace metal and isotope records to assess downcore diagenetic alterations. We consider a range of scenarios for recalculating SST from published Mg/Ca datasets and consider site-specific age models associated with each. We provide modern snapshot of the surface ocean salinity alongside locations of key study sites to consider past changes in salinity across the middle Miocene. We compare gradients in planktic and benthic carbon isotopes to explore changes in productivity at ODP site 761. All data are presented in the Supplementary Tables.

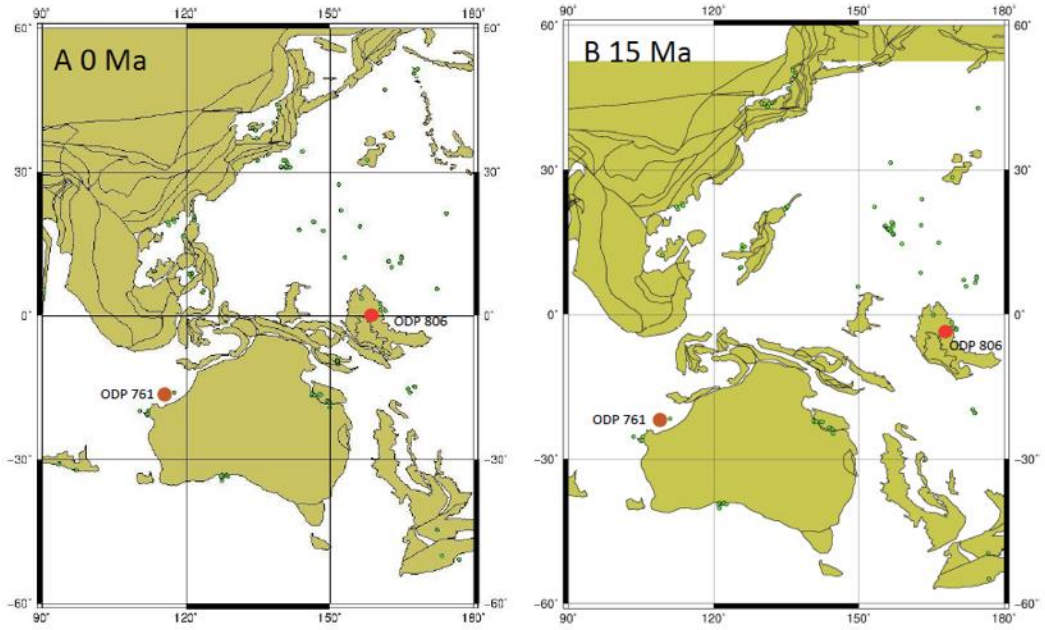

Figure S1 Locations of sites discussed in this study. Paleo-latitude and geographic reconstruction for (A) 0 and (B) 15.0 Ma were generated from http://www.odsn.de/ Green circles represent ODP sites with site 806 and 761 highlighted in red and brown circles, respectively. Note the long-term northward migration of both ODP sites 806 and 761.

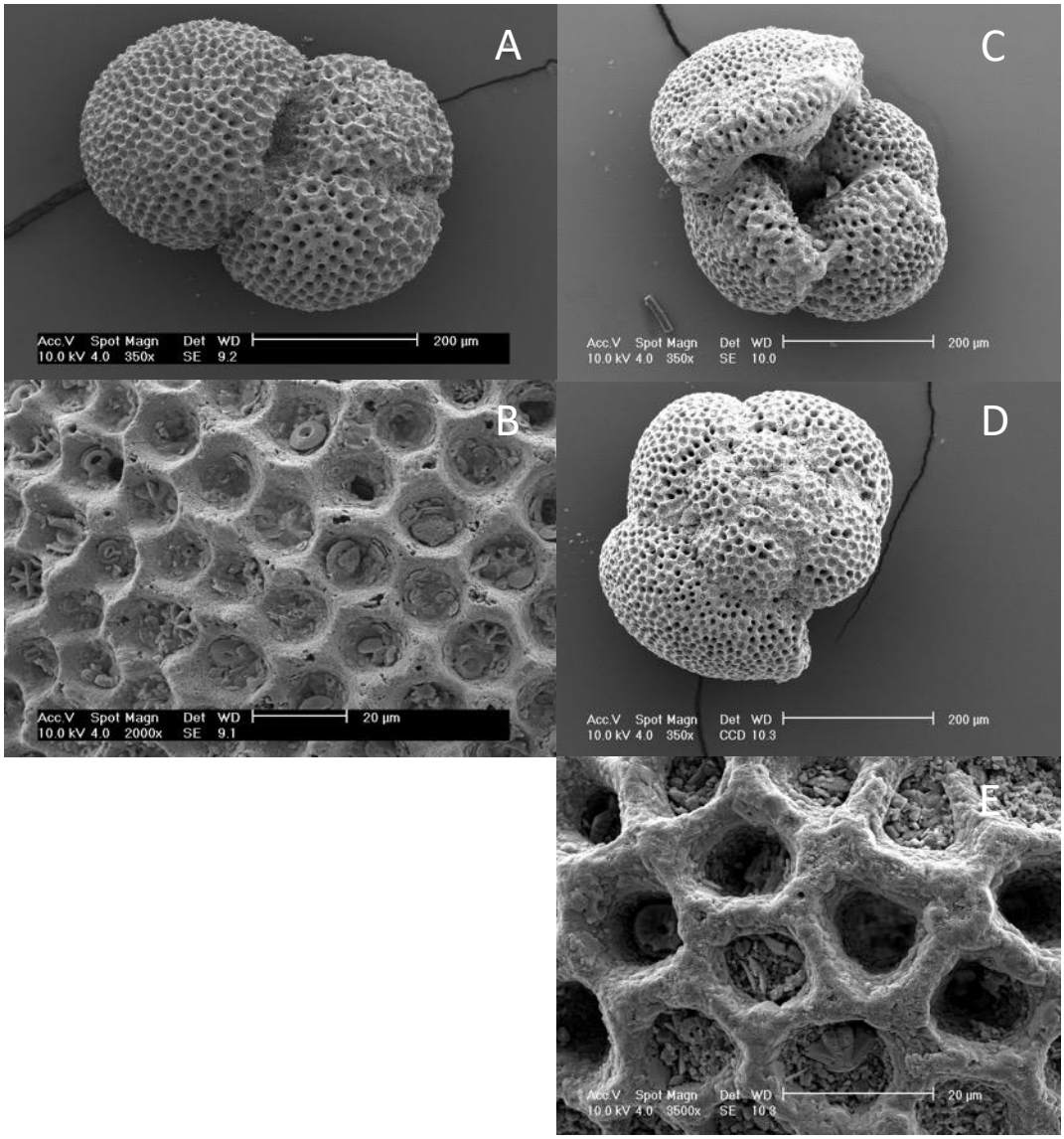

Figure S2 SEM images of species used in this study. (A) Whole test of *T. trilobus* from ODP 761B 05-05 103-105 cm 300-355 µm size fraction (39.73 m below seafloor); (B) Wall structure of *T. trilobus* test showing original microstructure; (C-D) Whole test spiral and umbilical side view of *D. altispira*; (E) Wall structure of *D. altispira* test.

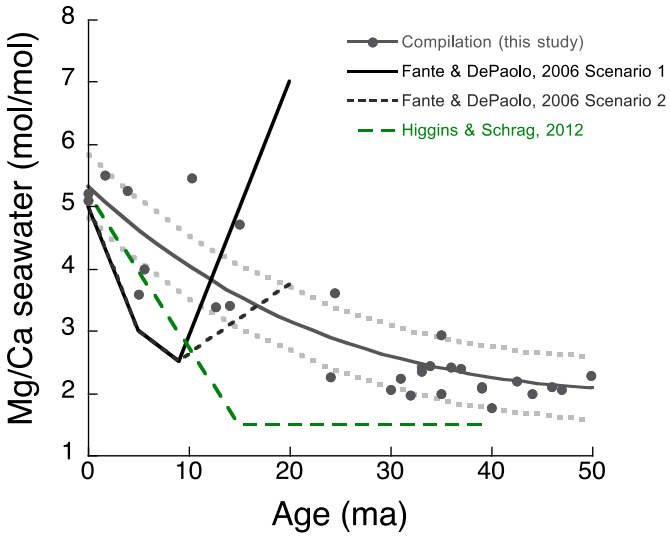

Figure S3 Various Mg/Ca seawater reconstructions from a compilation of published proxy data (this study) and porewater modeling (Fantle & DePaolo, 2006; Higgins & Schrag, 2012). Note a linear fit was used in lieu of the model output for FD06 and HS12 to look at long-term trends and impact on Mg/Ca-SST trends and consider two scenarios for FD06 as presented in Fante & DePaola, 2006).

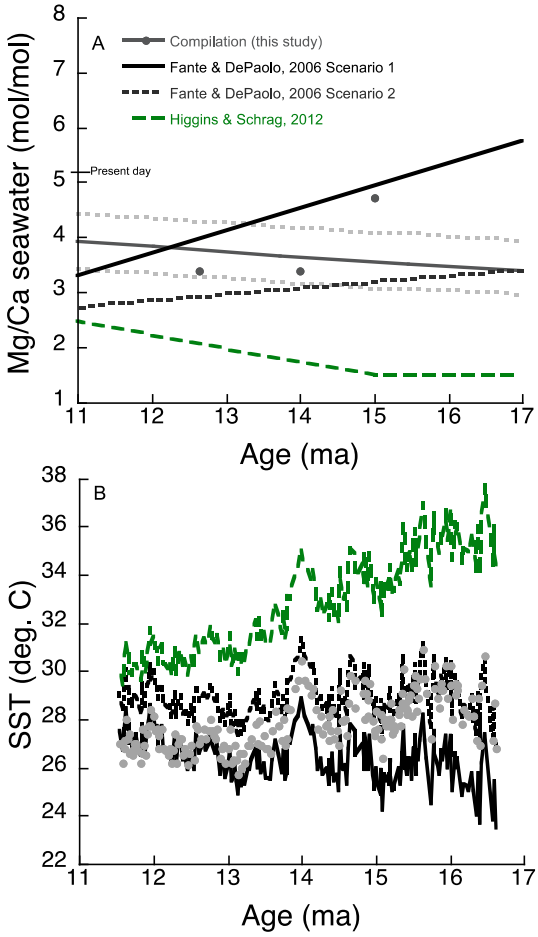

Figure S4 (A) Various Miocene Mg/Ca seawater estimates and (B) corresponding estimated *T. trilobus* Mg/Ca-SST using the Gray and Evans (2019) equation as specified in the manuscript.

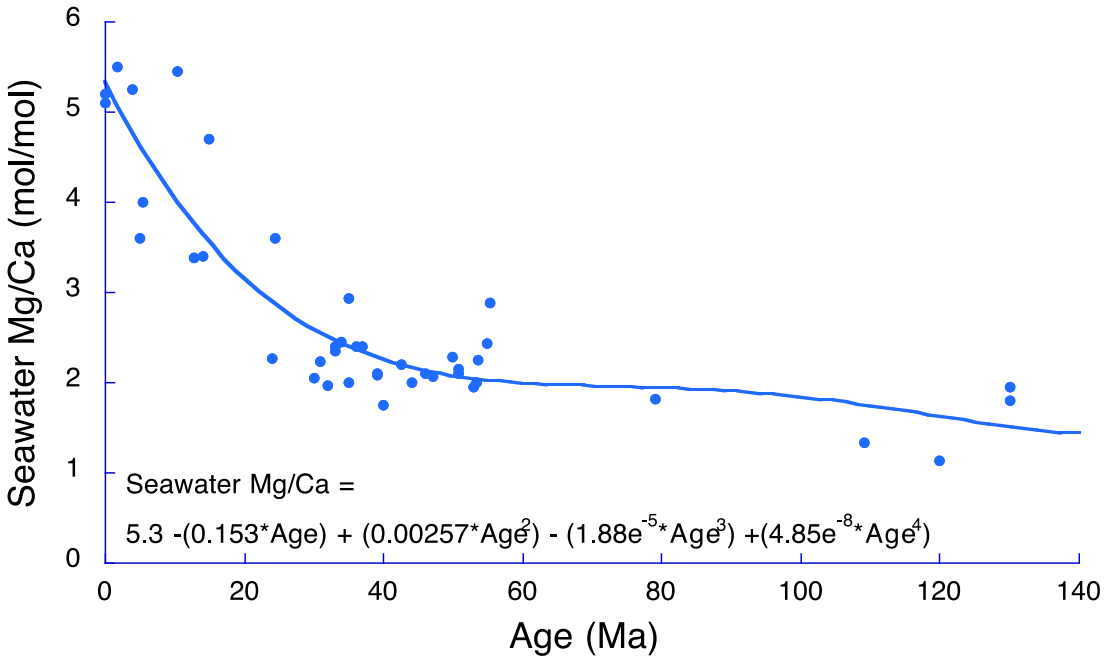

Figure S5 Fourth order polynomial curve fit through compiled seawater Mg/Ca proxy records based on fluid inclusions, calcite veins, echinoderms, and large benthic foraminifera (Dickson, 2002, Horita et al., 2002, Brennan et al., 2013; Coggon et al., 2010; Rausch et al., 2013; Evans et al., 2018).

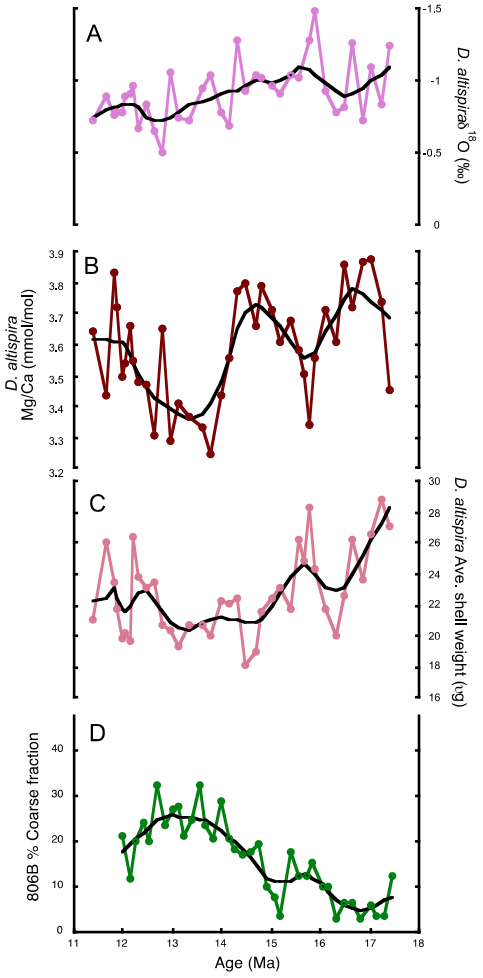

Figure S6 ODP site 806 *D. altispira* $\delta^{18}O_p$ (A) and Mg/Ca (B) records plotted against (C) average shell weight and (D) percent coarse fraction. Solid black lines represent 25% weighted fit line.

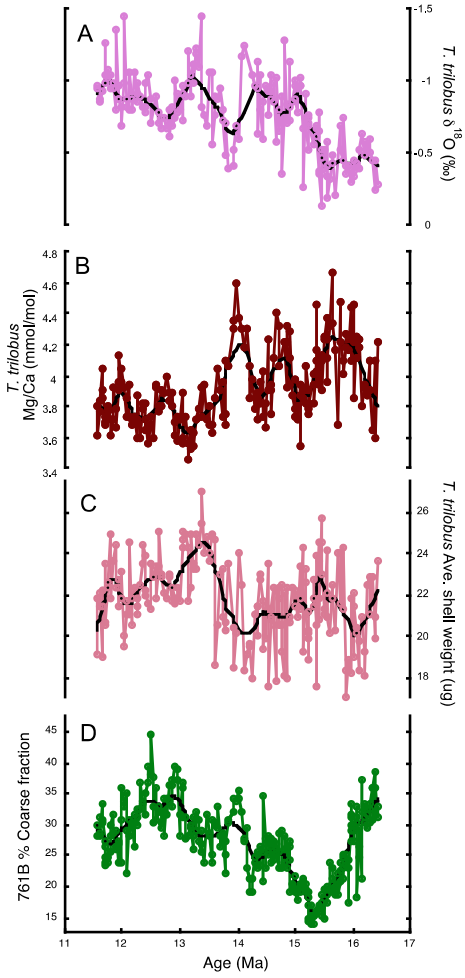

Figure S7 ODP Site 761 (A) *T. trilobus* $\delta^{18}O_p$ and (B) Mg/Ca ratios (Sosdian et al., 2020) records plotted alongside (C) average shell weight and (D) coarse fraction. Solid black lines represent 10% weighted fit line.

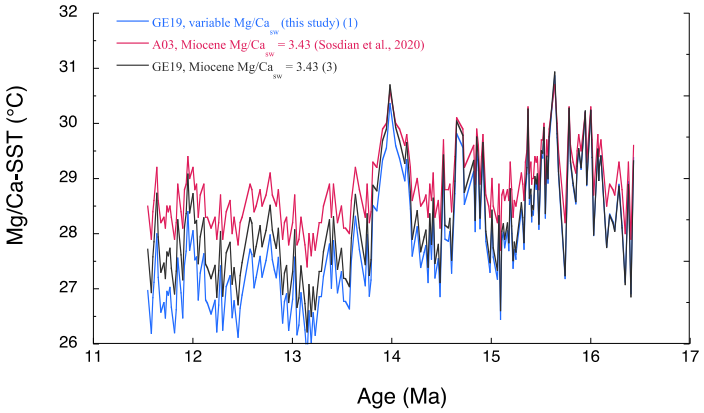

Figure S8 ODP site 761 Mg/Ca-SST reconstructions for a range of scenarios as follows (1) application of Gray and Evans (2019)(GE19) multi-variable regression accounting for changes in Mg/Ca_{sw}, (2) application of Anand et al., (2003) *T. sacculifer* Mg/Ca-T equation with Miocene Mg/Ca_{sw} value of 3.43 mmol/mol as estimated in Sosdian et al., (2020), and (3) application of Gray and Evans (2019) multi-variable regression with constant Miocene Mg/Ca_{sw} value of 3.43 mmol/mol.

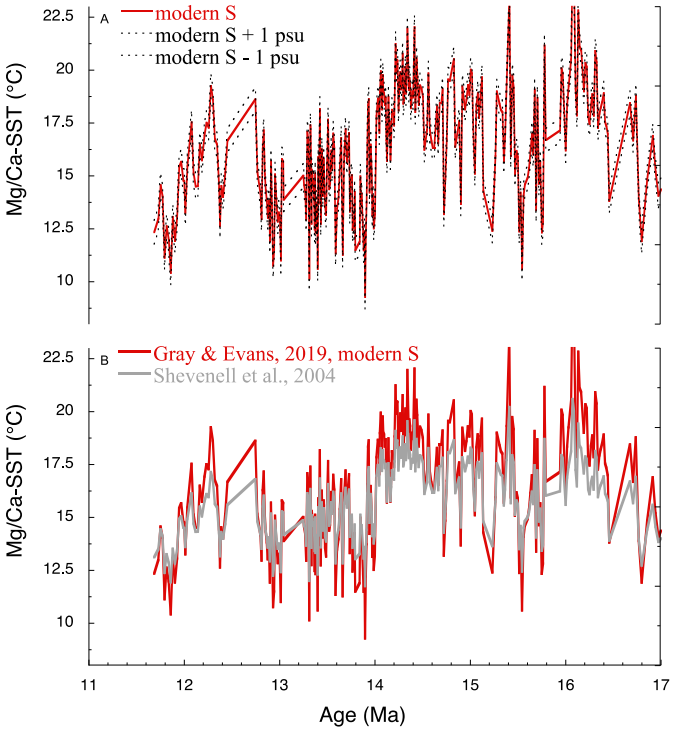

Figure S9 ODP site 1171 Mg/Ca-SST reconstructions derived from the sensitivity analysis (A) SST estimates derived from ODP site 1171 *G. bulloides* Mg/Ca with varying salinity scenarios (constant modern, constant modern +1 PSU, constant modern -1 PSU); (B) SST estimates derived using the Mg/Ca-T equation from Mashiotta et al., (1999) and assuming modern values for Mg/Ca_{sw} (Shevenell et al., 2004) and using Gray and Evans (2019) multi-variable regression accounting for changes in pH, salinity, and Mg/Ca_{sw}.

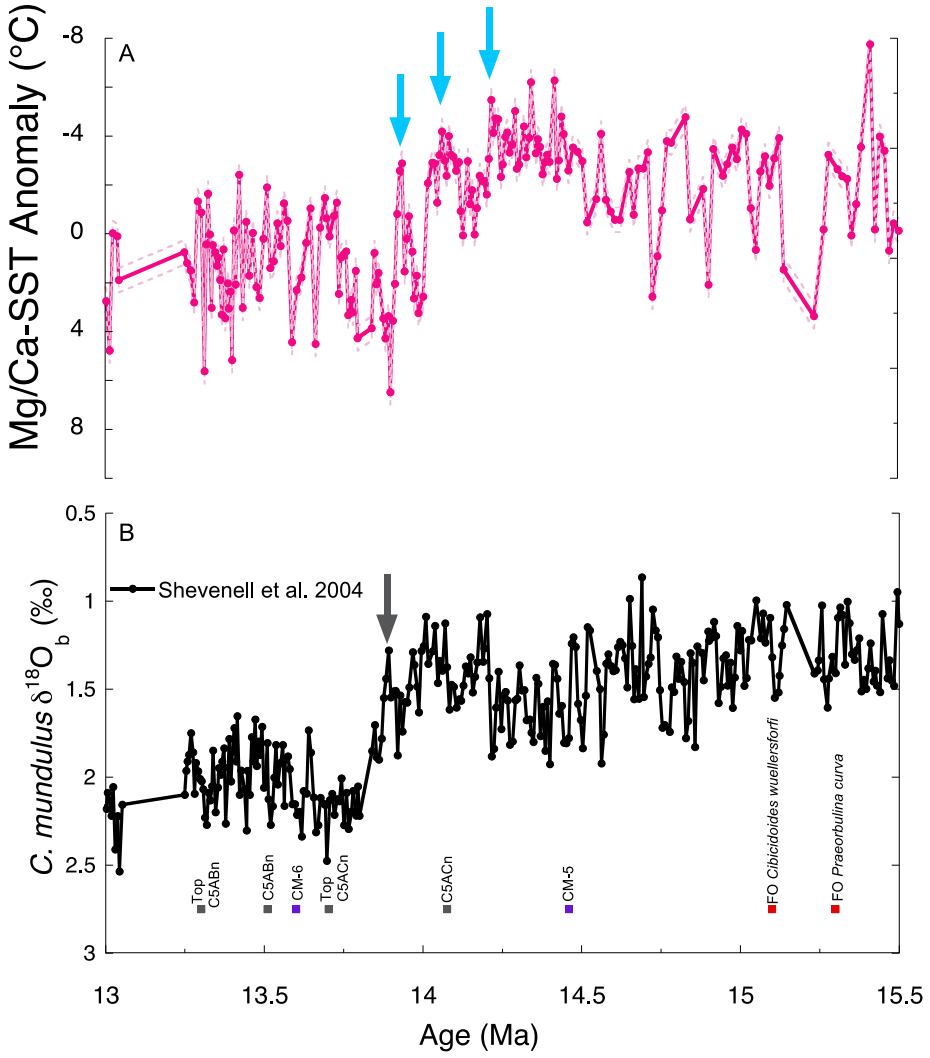

Figure S10 ODP Site 1171 (A) Mg/Ca-derived SST anomaly (calculated from record of Shevenell et al., (2004) and (B) benthic foraminiferal oxygen isotope records. Datums used in the age model are shown by colored squares (biostratigraphic datums-red squares, isotopic datums-purple squares, magnetostratigraphic datums-grey squares; Shevenell & Kennett, 2004). Blue arrows show major cooling steps in the Southern Ocean (Shevenell et al., 2004). Initial surface cooling step follows CM-5, but precedes magnetostratigraphic datum C5ACn, isotope event CM6 and the glaciation step (grey arrow).

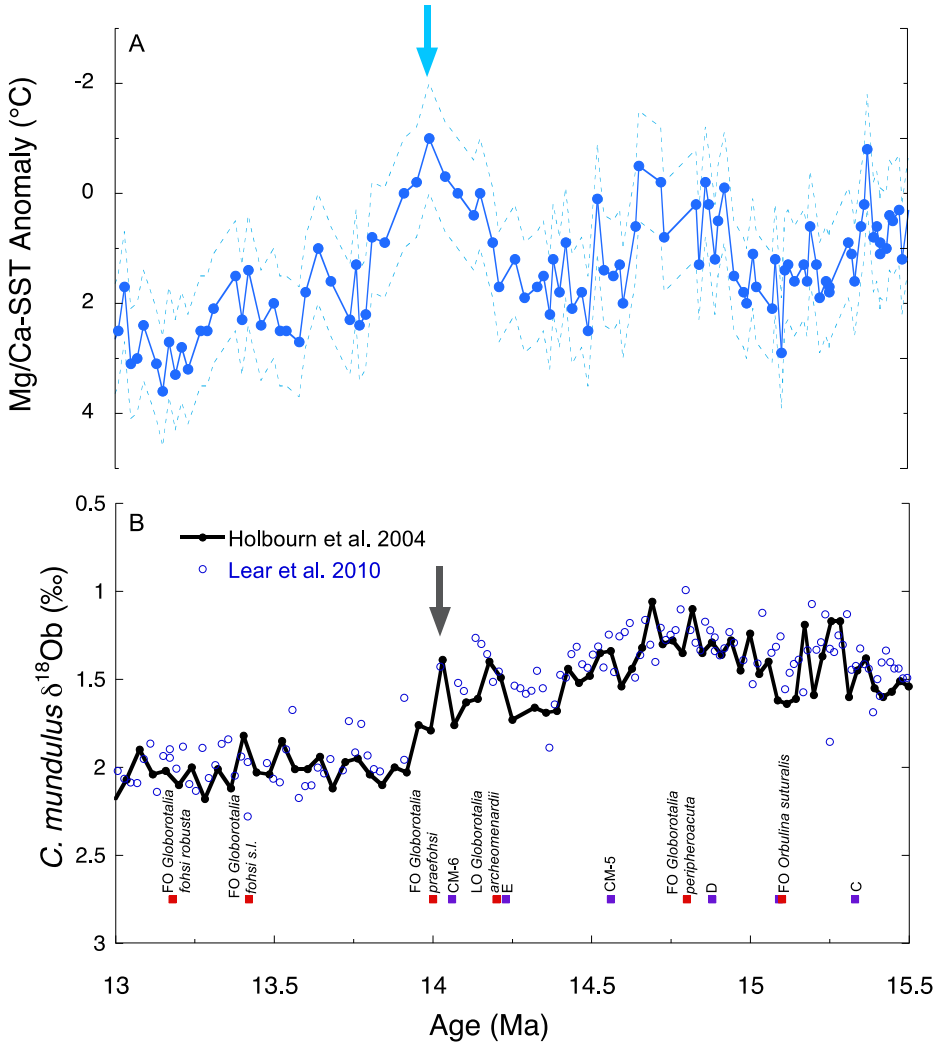

Figure S11 ODP Site 761 (A) Mg/Ca-derived SST anomaly (this study) and (B) benthic foraminiferal oxygen isotope records (Holbourn et al., 2004; Lear et al., 2010). Datums used in ODP Site 761 age model are shown by colored squares (biostratigraphic datums-red squares, isotopic datums-purple squares). Major MMCT surface cooling is shown by blue arrow, and occurs in step with CM6 and the main glaciation step (grey arrow).

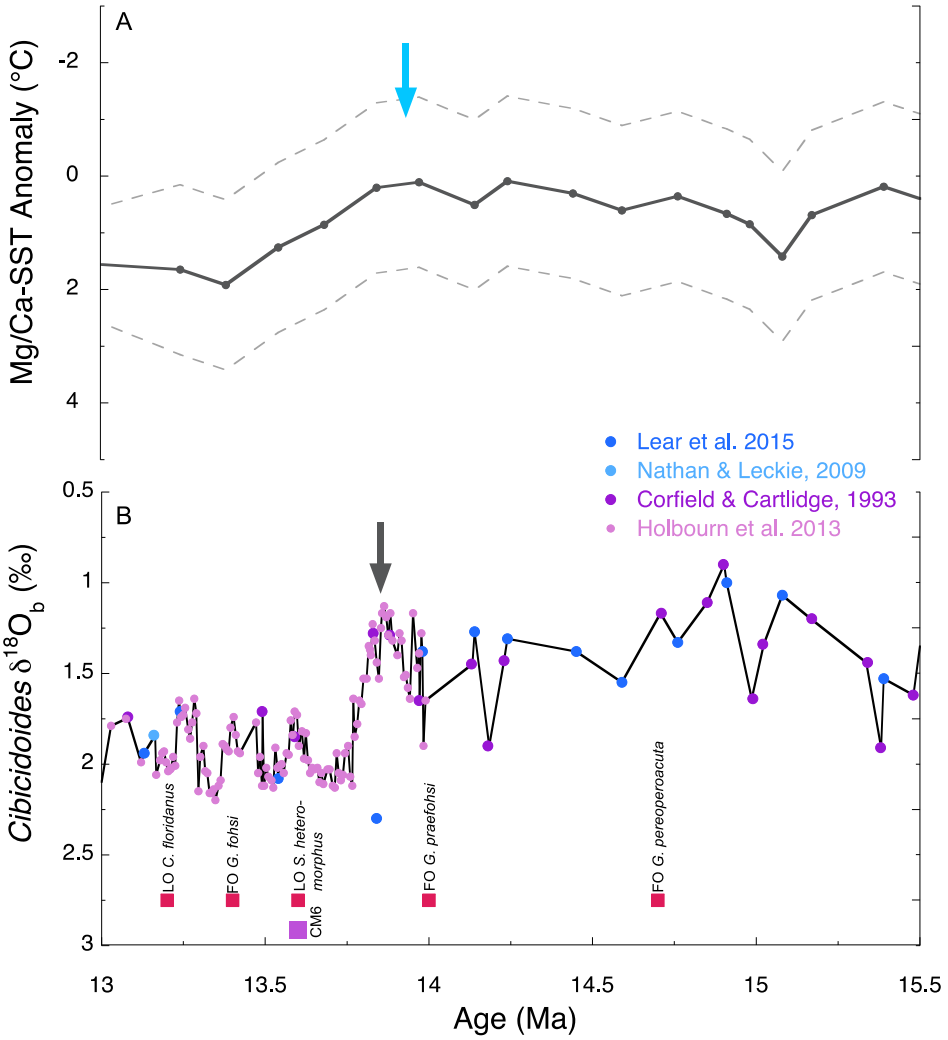

Figure S12 ODP Site 806 (A) Mg/Ca-derived SST anomaly (this study) and (B) benthic foraminiferal oxygen isotope records (Corfield and Cartlidge, 1983; Nathan and Leckie, 2009; Holbourn et al., 2013; Lear et al., 2015). Datums used in ODP Site 806 age model are marked by colored squares (biostratigraphic datums-red squares, isotopic datums-purple squares, magnetostratigraphic datums-gray squares). Cooling (blue arrow) and glaciation step (grey arrow) are marked in each record. Note CM6 isotope datum was not used in Lear et al., (2015) age model.

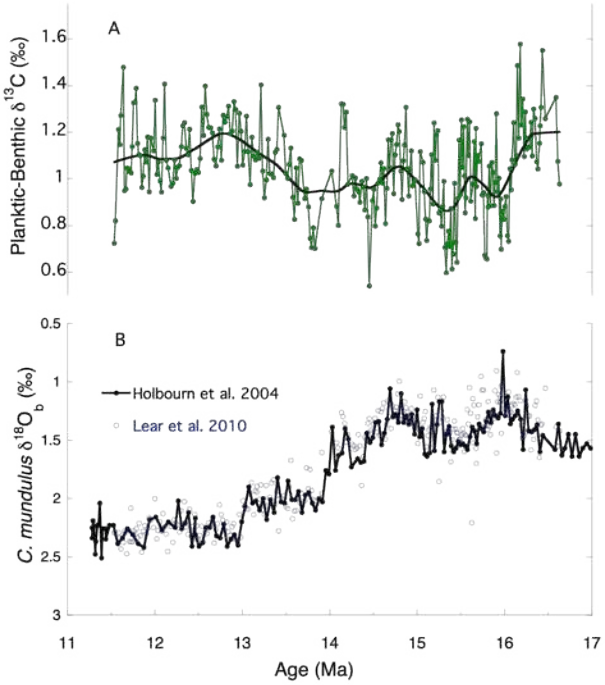

Figure S13 (A) $\delta^{13}C$ difference between planktonic (*T. trilobus;* Sosdian et al., 2020) and benthic foraminifera (*Cibicidoides sp*.; Holbourn et al., 2004; Lear et al., 2010) indicative of productivity at site 761 in the tropical Indian Ocean alongside the (b) compiled $\delta^{18}Ob$ records from ODP site 761 (Holbourn et al., 2004; Lear et al., 2004). Note more positive $\delta^{13}C$ values indicate more productivity.

Supplementary Tables

Supplementary Table S1 Datums used in Age Models for ODP Sites 761, 806 and 1171 across the Middle Miocene Climate Transition (13-15.5 Ma).

ODP site 761

Datum	Age (Ma)	Datum Type	Reference
FO *Globorotalia fohsi robusta*	13.18	Biostratigraphic	Holbourn et al. 2004
FO *Globorotalia fohsi s.l.*	13.42	Biostratigraphic	Holbourn et al. 2004
CM6	14.06	Isotopic	Holbourn et al. 2004
FO *Globorotalia praefohsi*	14	Biostratigraphic	Holbourn et al. 2004
LO *Globorotalia archeomenardii*	14.2	Biostratigraphic	Holbourn et al. 2004
E	14.23	Isotopic	Holbourn et al. 2004
CM5	14.56	Isotopic	Holbourn et al. 2004
D	14.88	Isotopic	Holbourn et al. 2004
FO *Globorotalia peripheroacuta*	14.8	Biostratigraphic	Holbourn et al. 2004
FO *Orbulina suturalis*	15.1	Biostratigraphic	Holbourn et al. 2004

ODP site 806

Datum	Age (Ma)	Datum Type	Reference
FO *G. fohsi*	13.4	Biostratigraphic	Lear et al. 2015
LO *C. floridanus*	13.2	Biostratigraphic	Lear et al. 2015
LO *S. heteromorphus*	13.6	Biostratigraphic	Lear et al. 2015
FO G. *praefohsi*	14.0	Biostratigraphic	Lear et al. 2015
FO G. *peripheroacuta*	14.7	Biostratigraphic	Lear et al. 2015

ODP site 1171

Datum	Age (Ma)	Datum Type	Reference
Top C5ABn	13.302	Magneto	Shevenell & Kennett, 2004
C5ABn	13.51	Magneto	Shevenell & Kennett, 2004
CM6	13.6	Isotopic	Shevenell & Kennett, 2004
Top C5ACn	13.703	Magneto	Shevenell & Kennett, 2004
C5ACn	14.076	Magneto	Shevenell & Kennett, 2004
CM5	14.46	Isotopic	Shevenell & Kennett, 2004
FO *Orbulina suturalis (F)*	15.1	Biostratigraphic	Shevenell & Kennett, 2004

Supplementary Table S2 *D. Altispira* Mg/Ca and oxygen isotope data at ODP site 806.

Site-Hole	Core	Sect	Interval (cm)		Depth (MCD)	Age (Ma)	Mg/Ca (mmol/mol)	*D. altispira* δ^{18}O (‰)
806B	43	2	80	85	399.8	11.3	3.64	-0.73
806B	44	2	83	87	409.52	11.6	3.44	-0.89
806B	44	5	93	95	414.13	11.7	3.83	-0.76
806B	44	6	113.5	115.5	415.835	11.8	3.72	-0.78
806B	45	2	92	97	419.32	11.9	3.50	-0.78
806B	45	3	76	78	420.66	11.9	3.54	-0.90
806 B	45	5	81	86	423.71	12.0	3.66	-0.91
806B	45	6	108.5	110.5	425.485	12.0	3.55	-0.96
806 B	46	2	82	87	428.82	12.1	3.48	-0.68
806B	46	5	82	87	433.32	12.3	3.47	-0.84

806 B	47	2	70	76	438.3	12.4	3.31	-0.66
806 B	47	5	38	43	442.48	12.5	3.65	-0.50
806 B	48	2	64	69	447.94	12.7	3.29	-1.06
806 B	48	5	60	65	452.4	12.8	3.41	-0.74
806B	49	2	68	73	457.68	13.0	3.37	-0.73
806 B	50	2	70	75	465.8	13.2	3.33	-0.95
806B	50	5	80	85	470.4	13.4	3.25	-1.05
806 B	51	2	68	73	475.48	13.5	3.44	-0.78
806 B	51	5	80	85	480.1	13.7	3.56	-0.70
806 B	52	2	88	93	484.98	13.8	3.77	-1.29
806 B	52	5	77	82	489.37	14.0	3.80	-0.94
806 B	53	2	71	76	494.51	14.1	3.66	-1.04
806 B	53	4	80	85	497.6	14.2	3.79	-1.02
806 B	54	2	71	76	504.11	14.4	3.71	-0.97
806 B	54	5	66	68	508.56	14.6	3.61	-0.92
806 B	55	2	80	85	513.9	14.8	3.68	-1.05
806 B	55	5	102	104	518.4	14.9	3.58	-1.02
806B	55	7	19	21	520.79	15.0	3.51	
806 B	56	2	87	92	523.67	15.1	3.34	-1.29
806 B	56	4	69	74	526.49	15.2	3.56	-1.48
806 B	57	2	70	75	533.1	15.4	3.71	-0.93
806 B	57	5	80	85	537.7	15.5	3.61	-0.79

806 B	58	2	70	75	542.7	15.7	3.86	-0.82
806 B	58	5	75	80	547.25	15.9	3.72	-1.26
806 B	59	2	70	75	552.4	16.0	3.87	-0.72
806 B	59	5	80	85	557	16.2	3.88	-1.09
806 B	60	2	80	85	562.2	16.3	3.74	-0.83
806 B	60	5	36	41	566.26	16.5	3.45	-1.24

Supplementary Table S3 *T. trilobus* oxygen isotope data at ODP site 761.

Site-Hole	Core	Section	Interval (cm)	MBSF	MCD	Age (Ma)	*T. trilobus* $\delta^{18}O$ (‰)
761B	5	2	88-90	35.08	35.58	11.55	-0.96
761B	5	2	103-105	35.23	35.73	11.59	-0.94
761B	5	2	108-110	35.28	35.78	11.60	-0.86
761B	5	2	113-115	35.33	35.83	11.61	-0.88
761B	5	2	123-125	35.43	35.93	11.64	-0.94
761B	5	2	128-130	35.48	35.98	11.65	-0.93
761B	5	2	138-140	35.58	36.08	11.68	-1.04
761B	5	2	148-150	35.68	36.18	11.71	-1.27
761B	5	3	3-5	35.73	36.23	11.73	-0.99
761B	5	3	8-10	35.78	36.28	11.74	-1.07
761B	5	3	13-15	35.83	36.33	11.76	-1.08
761B	5	3	18-20	35.88	36.38	11.77	-1.03
761B	5	3	23-25	35.93	36.43	11.79	-1.05

761B	5	3	33-35	36.03	36.53	11.82	-0.96
761B	5	3	38-40	36.08	36.58	11.84	-0.95
761B	5	3	43-45	36.13	36.63	11.85	-0.99
761B	5	3	53-55	36.23	36.73	11.88	-0.80
761B	5	3	58-60	36.28	36.78	11.90	-1.36
761B	5	3	63-65	36.33	36.83	11.92	-0.87
761B	5	3	68-70	36.38	36.88	11.94	-0.97
761B	5	3	73-75	36.43	36.93	11.95	-0.87
761B	5	3	78-80	36.48	36.98	11.97	-0.82
761B	5	3	88-90	36.58	37.08	12.00	-0.70
761B	5	3	93-95	36.63	37.13	12.02	-0.99
761B	5	3	98-100	36.68	37.18	12.04	-1.45
761B	5	3	103-105	36.73	37.23	12.06	-0.87
761B	5	3	108-110	36.78	37.28	12.08	-0.81
761B	5	3	118-120	36.88	37.38	12.11	-0.80
761B	5	3	123-125	36.93	37.43	12.13	-1.06
761B	5	3	128-130	36.98	37.48	12.15	-0.87
761B	5	3	138-140	37.08	37.58	12.19	-0.80
761B	5	3	148-150	37.18	37.68	12.22	-1.06
761B	5	4	3-5	37.23	37.73	12.24	-0.85
761B	5	4	8-10	37.28	37.78	12.26	-0.92
761B	5	4	13-15	37.33	37.83	12.28	-1.00
761B	5	4	18-20	37.38	37.88	12.30	-0.89
761B	5	4	28-30	37.48	37.98	12.34	-0.81
761B	5	4	38-40	37.58	38.08	12.38	-0.78

761B	5	4	43-45	37.63	38.13	12.40	-0.81
761B	5	4	48-50	37.68	38.18	12.42	-0.98
761B	5	4	58-60	37.78	38.28	12.46	-1.05
761B	5	4	63-65	37.83	38.33	12.48	-0.88
761B	5	4	68-70	37.88	38.38	12.50	-0.70
761B	5	4	88-90	38.08	38.58	12.58	-0.90
761B	5	4	98-100	38.18	38.68	12.62	-0.72
761B	5	4	103-105	38.23	38.73	12.64	-0.78
761B	5	4	113-115	38.33	38.83	12.68	-0.67
761B	5	4	118-120	38.38	38.88	12.70	-0.74
761B	5	4	128-130	38.48	38.98	12.74	-0.75
761B	5	4	138-140	38.58	39.08	12.78	-0.66
761B	5	4	143-145	38.63	39.13	12.80	-0.80
761B	5	4	148-150	38.68	39.18	12.82	-0.62
761B	5	5	3-5	38.73	39.23	12.84	-0.83
761B	5	5	8-10	38.78	39.28	12.86	-0.69
761B	5	5	18-20	38.88	39.38	12.90	-0.75
761B	5	5	23-25	38.93	39.43	12.92	-1.01
761B	5	5	28-30	38.98	39.48	12.95	-0.79
761B	5	5	33-35	39.03	39.53	12.97	-0.92
761B	5	5	43-45	39.13	39.63	13.01	-0.80
761B	5	5	48-50	39.18	39.68	13.03	-0.96
761B	5	5	53-55	39.23	39.73	13.05	-0.73
761B	5	5	58-60	39.28	39.78	13.07	-0.92
761B	5	5	63-65	39.33	39.83	13.09	-0.89

761B	5	5	73-75	39.43	39.93	13.13	-0.99
761B	5	5	78-80	39.48	39.98	13.15	-1.22
761B	5	5	83-85	39.53	40.03	13.17	-0.90
761B	5	5	88-90	39.58	40.08	13.19	-1.05
761B	5	5	93-95	39.63	40.13	13.21	-1.11
761B	5	5	98-100	39.68	40.18	13.23	-0.98
761B	5	5	108-110	39.78	40.28	13.27	-1.23
761B	5	5	113-115	39.83	40.33	13.29	-1.20
761B	5	5	118-120	39.88	40.38	13.32	-1.10
761B	5	5	133-135	40.03	40.53	13.38	-1.45
761B	5	5	138-140	40.08	40.58	13.40	-0.82
761B	5	5	143-145	40.13	40.63	13.42	-0.77
761B	5	6	3-5	40.23	40.73	13.46	-0.70
761B	5	6	18-20	40.38	40.88	13.52	-1.05
761B	5	6	23-25	40.43	40.93	13.54	-1.07
761B	5	6	28-30	40.48	40.98	13.56	-0.57
761B	5	6	38-40	40.58	41.08	13.60	-0.76
761B	5	6	43-45	40.63	41.13	13.62	-0.89
761B	5	6	48-50	40.68	41.18	13.64	-0.87
761B	5	6	58-60	40.78	41.28	13.68	-0.96
761B	5	6	73-75	40.93	41.43	13.74	-0.80
761B	5	6	78-80	40.98	41.48	13.76	-0.73
761B	5	6	83-85	41.03	41.53	13.78	-0.49
761B	5	6	93-95	41.13	41.63	13.81	-0.70
761B	5	6	113-115	41.23	41.73	13.85	-0.39

761B	5	6	118-120	41.38	41.88	13.91	-0.41
761B	5	6	128-130	41.48	41.98	13.95	-0.53
761B	5	6	138-140	41.58	42.08	13.99	-0.70
761B	5	7	3-5	41.73	42.23	14.04	-0.60
761B	5	7	13-15	41.83	42.33	14.08	-1.17
761B	5	7	28-30	41.98	42.48	14.13	-1.25
761B	5	CC	8-10	42.32	42.82	14.26	-1.05
761B	5	CC	18-20	42.42	42.92	14.29	-0.97
761B	5	CC	28-30	42.52	43.02	14.33	-0.94
761B	5	CC	33-35	42.57	43.07	14.35	-1.13
761B	6	1	3-5	42.23	43.13	14.37	-0.64
761B	6	1	8-10	42.28	43.18	14.38	-1.04
761B	6	1	13-15	42.33	43.23	14.40	-0.81
761B	6	1	18-20	42.38	43.28	14.42	-0.60
761B	6	1	23-25	42.43	43.33	14.44	-0.85
761B	6	1	38-40	42.58	43.48	14.49	-0.97
761B	6	1	48-50	42.68	43.58	14.52	-0.93
761B	6	1	53-55	42.73	43.63	14.54	-0.76
761B	6	1	63-65	42.83	43.73	14.57	-1.03
761B	6	1	68-70	42.88	43.78	14.59	-0.88
761B	6	1	73-75	42.93	43.83	14.60	-0.93
761B	6	1	78-80	42.98	43.88	14.62	-0.86
761B	6	1	83-85	43.03	43.93	14.64	-0.98
761B	6	1	88-90	43.08	43.98	14.65	-0.59
761B	6	1	98-100	43.18	44.08	14.69	-1.02

761B	6	1	103-105	43.23	44.13	14.70	-0.65
761B	6	1	108-110	43.28	44.18	14.72	-0.80
761B	6	1	113-115	43.33	44.23	14.73	-0.72
761B	6	1	118-120	43.38	44.28	14.75	-0.73
761B	6	1	123-125	43.43	44.33	14.77	-0.90
761B	6	1	128-130	43.48	44.38	14.78	-0.35
761B	6	1	138-140	43.58	44.48	14.81	-0.74
761B	6	1	143-145	43.63	44.53	14.83	-1.29
761B	6	1	148-150	43.68	44.58	14.84	-0.70
761B	6	2	3-5	43.73	44.63	14.86	-0.84
761B	6	2	8-10	43.78	44.68	14.87	-0.75
761B	6	2	13-15	43.83	44.73	14.89	-0.74
761B	6	2	18-20	43.88	44.78	14.90	-1.14
761B	6	2	23-25	43.93	44.83	14.92	-0.83
761B	6	2	33-35	44.03	44.93	14.95	-0.85
761B	6	2	43-45	44.13	45.03	14.98	-0.97
761B	6	2	48-50	44.18	45.08	14.99	-1.00
761B	6	2	53-55	44.23	45.13	15.01	-0.87
761B	6	2	58-60	44.28	45.18	15.02	-0.79
761B	6	2	73-75	44.43	45.33	15.07	-0.96
761B	6	2	78-80	44.48	45.38	15.08	-0.97
761B	6	2	83-85	44.53	45.43	15.10	-1.02
761B	6	2	88-90	44.58	45.48	15.11	-0.97
761B	6	2	93-95	44.63	45.53	15.12	-0.67
761B	6	2	98-100	44.68	45.58	15.14	-0.26

761B	6	2	108-110	44.78	45.68	15.17	-0.91
761B	6	2	113-115	44.83	45.73	15.18	-0.76
761B	6	2	118-120	44.88	45.78	15.19	-0.70
761B	6	2	123-125	44.93	45.83	15.21	-0.52
761B	6	2	128-130	44.98	45.88	15.22	-0.77
761B	6	2	133-135	45.03	45.93	15.24	-0.75
761B	6	2	138-140	45.08	45.98	15.25	-0.70
761B	6	2	138-140	45.08	45.98	15.25	-0.70
761B	6	3	13-15	45.33	46.23	15.32	-0.56
761B	6	3	28-30	45.48	46.38	15.36	-0.67
761B	6	3	33-35	45.53	46.43	15.37	-0.70
761B	6	3	38-40	45.58	46.48	15.39	-0.62
761B	6	3	43-45	45.63	46.53	15.40	-0.37
761B	6	3	46-48	45.66	46.56	15.41	-0.78
761B	6	3	48-50	45.68	46.58	15.41	-0.66
761B	6	3	53-55	45.73	46.63	15.43	-0.37
761B	6	3	58-60	45.78	46.68	15.44	-0.13
761B	6	3	63-65	45.83	46.73	15.45	-0.36
761B	6	3	68-70	45.88	46.78	15.47	-0.52
761B	6	3	73-75	45.93	46.83	15.48	-0.47
761B	6	3	83-85	46.03	46.93	15.51	-0.40
761B	6	3	88-90	46.08	46.98	15.52	-0.53
761B	6	3	93-95	46.13	47.03	15.53	-0.42
761B	6	3	98-100	46.18	47.08	15.55	-0.34
761B	6	3	103-105	46.23	47.13	15.56	-0.57

761B	6	3	108-110	46.28	47.18	15.57	-0.20
761B	6	3	113-115	46.33	47.23	15.59	-0.32
761B	6	3	133-135	46.53	47.43	15.64	-0.43
761B	6	3	143-145	46.63	47.53	15.67	-0.50
761B	6	3	148-150	46.68	47.58	15.68	-0.22
761B	6	4	38-40	47.08	47.98	15.79	-0.69
761B	6	4	43-45	47.13	48.03	15.80	-0.52
761B	6	4	53-55	47.23	48.13	15.83	-0.45
761B	6	4	63-65	47.33	48.23	15.85	-0.74
761B	6	4	68-70	47.38	48.28	15.87	-0.41
761B	6	4	73-75	47.43	48.33	15.88	-0.35
761B	6	4	83-85	47.53	48.43	15.91	-0.41
761B	6	4	98-100	47.68	48.58	15.95	-0.31
761B	6	4	118-120	47.88	48.78	16.00	-0.45
761B	6	4	123-125	47.93	48.83	16.02	-0.34
761B	6	4	128-130	47.98	48.88	16.03	-0.37
761B	6	4	146-148	48.16	49.06	16.08	-0.43
761B	6	4	148-150	48.18	49.08	16.09	-0.39
761B	6	5	3-5	48.23	49.13	16.10	-0.52
761B	6	5	23-25	48.43	49.33	16.16	-0.65
761B	6	5	33-35	48.53	49.43	16.19	-0.49
761B	6	5	43-45	48.63	49.53	16.22	-0.58
761B	6	5	50-52	48.7	49.6	16.25	-0.52
761B	6	5	63-65	48.83	49.73	16.29	-0.60
761B	6	5	73-75	48.93	49.83	16.32	-0.52

761B	6	5	83-85	49.03	49.93	16.35	-0.44
761B	6	5	93-95	49.13	50.03	16.38	-0.25
761B	6	5	100-102	49.2	50.1	16.41	-0.45
761B	6	5	108-110	49.28	50.18	16.43	-0.29

168
169
170
171
172
173
174
175
176
177
178
179
180
181
182
183